



# **Non-targeted Stressful Effects in Normal Human Fibroblast Cultures Exposed to Low Fluences of High Charge, High-Energy (HZE) Particles: Kinetics of Biologic Responses and Significance of Secondary Radiations.**

Géraldine Gonon, Jean-Emmanuel Groetz, Sonia M de Toledo, Roger W Howell, Michel Fromm, Edouard I Azzam

## **► To cite this version:**

Géraldine Gonon, Jean-Emmanuel Groetz, Sonia M de Toledo, Roger W Howell, Michel Fromm, et al.. Non-targeted Stressful Effects in Normal Human Fibroblast Cultures Exposed to Low Fluences of High Charge, High-Energy (HZE) Particles: Kinetics of Biologic Responses and Significance of Secondary Radiations.. Radiation Research, 2013, epub ahead of print. 10.1667/RR3017.1 . hal-00801993

**HAL Id: hal-00801993**

**<https://hal.science/hal-00801993>**

Submitted on 18 Mar 2013

**HAL** is a multi-disciplinary open access archive for the deposit and dissemination of scientific research documents, whether they are published or not. The documents may come from teaching and research institutions in France or abroad, or from public or private research centers.

L'archive ouverte pluridisciplinaire **HAL**, est destinée au dépôt et à la diffusion de documents scientifiques de niveau recherche, publiés ou non, émanant des établissements d'enseignement et de recherche français ou étrangers, des laboratoires publics ou privés.

1 **Non-Targeted Stressful Effects in Normal Human Fibroblast Cultures Exposed to**  
2 **Low Fluences of High Charge, High Energy (HZE) Particles: Kinetics of Biologic**  
3 **Responses and Significance of Secondary Radiations**

Géraldine Gonon<sup>a,b</sup>, Jean-Emmanuel Groetz<sup>b</sup>, Sonia M. de Toledo<sup>a</sup>, Roger W. Howell<sup>a</sup>,  
Michel Fromm<sup>b,1</sup> and Edouard I. Azzam<sup>a,2</sup>

<sup>a</sup>Department of Radiology, UMDNJ - New Jersey Medical School Cancer Center,  
Newark, NJ 07103, USA

<sup>b</sup>Laboratoire de Chimie Physique et Rayonnements - Alain Chambaudet (LCPR-AC),  
LRC CEA, UMR CNRS 6249 Chrono-Environnement, Université de Franche-Comté,  
Besançon, France

Running head: HZE-PARTICLE-INDUCED BYSTANDER EFFECTS

Key words: bystander effects, space exploration, radiation protection, hadron therapy,  
HZE ion fragmentation, secondary radiation

Manuscript Category: Regular Paper

Number of Pages: 44

Number of Figures: 6

Number Tables: 2

Supplementary Figures: 1; Supplementary Tables: 4

<sup>1,2</sup>Addresses for correspondence:

4 Edouard Azzam  
5 Department of Radiology  
6 UMDNJ – New Jersey Medical School  
7 Cancer Center  
8 205 South Orange Avenue  
9 Cancer Center Bldg. – Room F1212  
10 Newark, NJ 07103  
11 Phone: 973-972-5323  
12 Fax: 973-972-1865  
13 E-mail: azzamei@umdnj.edu

15 Michel Fromm  
16 Laboratoire de Chimie Physique et  
17 Rayonnements - Alain Chambaudet  
18 (LCPR-AC), LRC CEA, UMR CNRS  
19 6249 Chrono-Environnement  
20 Université de Franche-Comté,  
21 16 route de Gray  
22 F-25030 Besançon Cedex, France  
23 Phone: (0) 33 3 81 66 65 60  
24 Fax: (0) 33 3 81 66 65 22  
25 E-mail: michel.fromm@univ-fcomte.fr

## ABSTRACT

The induction of non-targeted stressful effects in cell populations exposed to low fluences of high charge (Z) and high energy (E) particles is relevant to estimates of the health risks of space radiation. We investigated the upregulation of stress markers in confluent normal human fibroblast cultures exposed to 1000 MeV/u iron ions (linear energy transfer (LET)  $\sim 151$  keV/ $\mu\text{m}$ ) or 600 MeV/u silicon ions (LET  $\sim 50$  keV/ $\mu\text{m}$ ) at mean absorbed doses as low as 0.2 cGy, wherein 1-3 % of the cells were targeted through the nucleus by a primary particle. Within 24 h post-irradiation, significant increases in the levels of phospho-TP53 (serine 15), p21<sup>Waf1</sup> (CDKN1A), HDM2, phospho-ERK1/2, protein carbonylation and lipid peroxidation were detected, which suggested participation in the stress response of cells not targeted by primary particles. This was supported by *in situ* studies that indicated greater increases in 53BP1 foci formation, a marker of DNA damage, than expected from the number of primary particle traversals. The effect was expressed as early as 15 min after exposure, peaked at 1 h, and decreased by 24 h. A similar tendency occurred after exposure of the cell cultures to 0.2 cGy of 3.7 MeV  $\alpha$  particles (LET  $\sim 109$  keV/ $\mu\text{m}$ ) that targets  $\sim 1.6$  % of nuclei, but not after 0.2 cGy from 290 MeV/u carbon ions (LET  $\sim 13$  keV/ $\mu\text{m}$ ) by which, on average,  $\sim 13$  % of the nuclei were hit, which highlights the importance of radiation quality in the induced effect. Simulations with the FLUKA multi-particle transport code revealed that fragmentation products, other than electrons, in cell cultures exposed to HZE particles comprise  $<1$  % of the absorbed dose. Further, the radial spread of dose due to secondary heavy ion fragments is confined to approximately 10-20  $\mu\text{m}$ . Thus, the latter are unlikely to significantly contribute to stressful effects in cells not targeted by primary HZE particles.

## INTRODUCTION

The ionizing radiation-induced bystander effect has been broadly defined as the induction of biological changes in cells not directly targeted by radiation (1). Stressful bystander effects have been extensively observed in cell populations where only a small fraction of the cells is targeted by high linear energy transfer (LET)  $\alpha$  particles. Induction of genetic alterations, including sister chromatid exchanges (2), mutations (3, 4), chromosomal aberrations (5) and micronuclei (6), changes in gene expression (7, 8), lethality (9) and neoplastic transformation (10, 11) have been observed in bystander cells of various lineages after exposure of other cells to  $\alpha$  particles. On the other hand, the characterization of bystander effects in cell cultures exposed to very low fluences of high charge (Z) and high energy (E) (HZE) particles, another type of high LET radiation, are only emerging, and conflicting data have been reported. In initial experiments with microbeam, stressful effects were shown to be transmitted from HZE-particle-irradiated cells to contiguous cells that were not targeted by the primary particle (12-14). In subsequent experiments whereby HZE-particle-irradiated cells were co-cultured with bystander cells in a manner that they only shared growth medium, stressful responses were also induced in the bystander cells and were similar in nature to those generated in the targeted cells (15-17). Furthermore, oxidative stress and DNA damage persisted in distant progeny of bystander cells that had been in contiguous co-culture with HZE-particle-irradiated cells (18, 19). However, other experiments involving the transfer of growth medium from irradiated cultures to recipient bystander cells present in a separate dish (9, 20), or the targeting of an exact number of cells in a population with energetic heavy ions from a microbeam (21) did not detect an effect with a variety of endpoints and

1 cell types. Several factors may underlie the absence of observable effects in these cases,  
2 including timing of endpoint measurement, dilution of the inducing factor and the  
3 metabolic state/redox environment of the recipient cells.

4 Providing clear evidence for HZE-particle-induced bystander effects is pertinent  
5 to space exploration during which astronauts are likely to be exposed to low fluences of  
6 energetic particles (22). To gain greater knowledge of HZE-particle-induced bystander  
7 effects, we investigated the expression of stress markers in density-inhibited normal  
8 human diploid fibroblast cultures exposed to low fluences of iron, silicon or carbon ions,  
9 and compared the results with those obtained in cultures exposed to low fluences of  
10  $\alpha$  particles. The data showed clear evidence for modulation of p53/p21<sup>Waf1</sup> and ERK1/2  
11 signaling in cultures exposed to doses as low as 0.2 cGy wherein only 1-3 % of nuclei are  
12 traversed by a primary particle track. An increase in protein carbonylation and lipid  
13 peroxidation was also detected at 24 h after exposure, suggesting that perturbations in  
14 oxidative metabolism contribute to the greater than expected stressful effects, based on  
15 microdosimetric considerations of the fraction of cells traversed by a primary particle. *In*  
16 *situ* immune-detection studies of 53BP1 foci formation, a marker that has been associated  
17 with DNA double strand breaks (23), together with the use of culture dishes where a  
18 solid-state nuclear track detector was fused to the glass bottom on which the cells grow,  
19 supported the involvement of cells not targeted by primary HZE particles in the response  
20 of cell cultures to radiation.

21 The microscopic structure of the primary HZE-particle-track is characterized by a  
22 high frequency of interactions with the target, which result in highly localized energy  
23 depositions (24, 25). Secondary radiations arise from interactions with atomic electrons

1 in target atoms and from fragmentation of the incident HZE particle and target nuclei.  
2 These secondaries are produced along the primary particle track and include energetic  
3 electrons ( $\delta$  rays), photons, protons, neutrons,  $\alpha$  particles and other heavier ions with  
4 different LET values. In contrast to  $\delta$  rays with a maximum range of  $\sim 0.1 \mu\text{m}$  that are  
5 produced in biological matter when traversed by the 2-10 MeV high-LET  $\alpha$  particles that  
6 are emitted during  $\alpha$  decay of radionuclides (26), the range of  $\delta$  rays produced following  
7 HZE particle-traversals can extend up to several cell diameters (27, 28), thereby  
8 potentially irradiating and contributing to biochemical changes in cells that are near those  
9 targeted by the primary particle track. In particular, protective mechanisms induced by  
10 low LET secondary radiations may mitigate stressful effects propagated from cells  
11 traversed by the primary particle (29). Alternatively, cells that were thought to be  
12 bystanders may be significantly irradiated by secondaries. To investigate whether  
13 secondary particles are a factor in apparent HZE-particle-induced bystander effects, the  
14 tracks of the secondaries were simulated with the multi-particle transport code FLUKA  
15 and absorbed doses received by the monolayer of cells adjacent to the targeted cells were  
16 assessed (30-32).

## 17 MATERIALS AND METHODS

### 18 *Cell culture*

19 AG1522 normal human diploid skin fibroblasts were obtained from the Genetic  
20 Cell Repository at the Coriell Institute for Medical Research. Cells at passage 10-12 were  
21 grown in Eagles' Minimum Essential Medium (MEM) (CellGro) containing 12.5 %  
22 (vol/vol) heat inactivated (30 min at 56 °C) fetal bovine serum (FBS) (Sigma),  
23 supplemented with 4 mM L-alanyl-L-glutamine (CellGro), 100 U/mL penicillin and

1 100 µg/mL streptomycin (CellGro). They were maintained in 37 °C humidified  
2 incubators in an atmosphere of 5 % CO<sub>2</sub> (vol/vol) in air. For experiments, cells were  
3 seeded at numbers that allowed them to reach the density-inhibited state within 5 days.  
4 They were then fed twice on alternate days, and experiments were initiated 48 h after the  
5 last feeding. Under these conditions, 95-98 % of cells were in G<sub>0</sub>/G<sub>1</sub> phase of the cell  
6 cycle. The synchronization of cells in G<sub>0</sub>/G<sub>1</sub> phase, by density-inhibition of growth,  
7 eliminates complications in interpretation of results that arise from changes in responses  
8 to ionizing radiation at different phases of the cell cycle (33).

9 For HZE-particle-irradiation, the cells were either grown in 25 cm<sup>2</sup> polystyrene  
10 flasks (Greiner) for Western blot analyses or in glass-bottomed flaskettes (Nalge Nunc  
11 International) for *in situ* detection of 53BP1 foci. Cells destined for α-particle-irradiation  
12 were seeded in stainless steel dishes with a circular 36-mm-diameter growing surface that  
13 consists of 1.5 µm-thick replaceable polyethylene terephthalate (PET). To facilitate cell  
14 attachment, the PET surface was precoated with FNC solution comprising fibronectin and  
15 collagen (AthenaES™), overlaid with 2 mL of MEM and incubated at 37 °C. After  
16 30 min, the medium was aspirated and the cells were seeded.

#### 17 *Culture dishes with nuclear track detector bottom and etching*

18 To identify cells irradiated by a primary particle, a 100 µm-thick polyallyl  
19 diglycol carbonate (PADC) plastic polymer (Tastrak™ from Track Analysis Systems  
20 Ltd., commonly known as Columbia Resin #39 or CR-39™ plastic) was grafted to the  
21 glass bottom of tissue culture dishes (Ibidi®) as shown in Supplementary Figure 1,  
22 Panel B. Upon cell fixation, the PADC was etched in 10 mol/L KOH at 37 °C for 3.5 h  
23 and the pits were visualized by light microscopy. *In situ* analyses of 53BP1 foci were

1 performed following etching. Images were obtained by switching from fluorescent to  
2 optical imaging and changing the focal plane. Monitoring of confluent cultures during a  
3 3 h period by confocal microscopy using a fixed high magnification field did not reveal  
4 any movement of the cells following exposure to mean absorbed doses of 0.1-0.3 cGy of  
5  $\alpha$  particles (34).

#### 6 *Irradiation and dosimetry*

7 Irradiation with 1000 MeV/u  $^{56}\text{Fe}^{26+}$ , 600 MeV/u  $^{28}\text{Si}^{14+}$  or 290 MeV/u  $^{12}\text{C}^{6+}$  with  
8 LET in liquid water of  $\sim 151$  keV/ $\mu\text{m}$ ,  $\sim 50$  keV/ $\mu\text{m}$  and  $\sim 13$  keV/ $\mu\text{m}$ , respectively, were  
9 performed at the NASA Space Radiation Laboratory (NSRL) at Brookhaven National  
10 Laboratory (Upton, NY) during 2008-2011. The monolayers were positioned  
11 perpendicularly to the beam in the plateau region of the Bragg curve, but were not  
12 stacked (profiles of the ions' Bragg curves can be accessed at [http://www.bnl.gov/](http://www.bnl.gov/medical/NASA/CAD/Bragg_Curves.asp)  
13 [medical/NASA/CAD/Bragg\\_Curves.asp](http://www.bnl.gov/medical/NASA/CAD/Bragg_Curves.asp)). The flasks were filled to capacity, 3 h prior to  
14 irradiation, with pH and temperature-equilibrated growth medium containing 20 %  
15 (vol/vol) conditioned medium that was harvested from confluent AG1522 cell cultures  
16 grown for 48 h. This ensured that, during the irradiation, deviation from 37 °C was  
17 attenuated and the cells were immersed in medium, which alleviates changes in  
18 osmolarity and partial oxygen tension. The latter parameters greatly affect the cellular  
19 responses to radiation (35, 36). The foam sample-holder produces minimal scatter or  
20 fragmentation of the incoming heavy ion beam ([www.bnl.gov/medical/NASA/CAD/](http://www.bnl.gov/medical/NASA/CAD/Sample_Holder_Layout.asp)  
21 [Sample\\_Holder\\_Layout.asp](http://www.bnl.gov/medical/NASA/CAD/Sample_Holder_Layout.asp)). Exposures to 0.2 or 1 cGy occurred at dose rates of 0.2 and  
22 1 cGy/min, respectively. The dose of 0.2 cGy was delivered in 3 or 4 spills at a  
23 minimum. Uniformity of the beam across the irradiated flasks was between 1 % and 5 %.



1 The dose just out of the beam (i.e. the beam-related background) is proportional to the  
2 beam dose and is on the order of 0.01 % of the dose in the beam. The background  
3 radiation due to activation depended on the preceding irradiation; in case our experiment  
4 was preceded by a 1 h exposure to the maximum rate of protons delivered at the NSRL,  
5 the  $\gamma$  ray dose that cells would receive would be at the rate of  $\sim 10^{-5}$  cGy/min. Sham-  
6 irradiated cell cultures served as control and were handled similarly as the test cultures.

7 Alpha-particle-irradiations were conducted with a 7.4 MBq  $^{241}\text{Am}$  collimated  
8 source housed in a helium-filled Plexiglas box located in a chamber at 37 °C with an  
9 atmosphere of 5 %  $\text{CO}_2$  (vol/vol) in air. To optimize uniformity of the beam, the source  
10 was mounted on a rotating platform (88 rpm) and the exit window was equipped with a  
11 beam delimiter. The uniformity was confirmed by etching PADC plastic exposed to the  
12 beam for 4 seconds. Cells were irradiated at a mean absorbed dose rate of 2 cGy/min, and  
13 irradiation of samples occurred from below through the PET growing surface. At the  
14 latter surface,  $\alpha$  particles had a measured mean energy of 3.7 MeV (0.92 MeV/u) with  
15 Full Width at Half Maximum (FWHM) of 0.5 MeV. The LET corresponding to a mean  
16 energy of 3.7 MeV is  $\sim 109$  keV/ $\mu\text{m}$  in liquid water. The irradiator box was fitted with a  
17 photographic shutter to allow accurate delivery of the desired mean absorbed dose (37).

18 The fluence  $\phi$  of HZE particles was determined by PMT/Scintillator-based  
19 dosimetry; it was then used to calculate the mean dose to the cell population according  
20 to the relation  $\phi$  (particles/ $\text{cm}^2$ ) =  $[D$  (cGy)  $\rho$  (g/ $\text{cm}^3$ )] /  $[1.602 \times 10^{-7}$  LET (keV/ $\mu\text{m}$ )],  
21 where  $D$  is the mean dose and  $\rho$  is the density. In case of  $\alpha$ -particle-irradiation, the  
22 fluence  $\phi$  for a fixed dose was estimated based on previous measurements (37). The  
23 average number of nuclear and cellular particle traversals was calculated by multiplying

1 the fluence with the average cross-section of an AG1522 cell nucleus (i.e.  $140 \mu\text{m}^2$  (7))  
2 or with the average cross-sectional area of an AG1522 whole cell (i.e.  $800 \mu\text{m}^2$  (34))  
3 measured in confluent cultures grown under similar conditions as in this study). The  
4 calculations of fluence were confirmed after etching of PADC. Estimates of the  
5 fractions of whole cells or nuclei traversed by a primary particle were calculated  
6 assuming Poisson statistics and are given in Table 1. These values were determined  
7 according to the method of Charlton and Sephton (38), where the probability P that a  
8 given target area is traversed by N particles is given by  $P(N) = e^{-x} x^N / N!$  with x being  
9 the product of the fluence and the target cross-sectional area (nucleus or whole cell).

#### 10 *Secondary radiations*

11 In this work, for studies of *in situ* detection of 53BP1 foci, the HZE particles  
12 traversed first the soda-lime glass bottom of the flaskettes before reaching the cells and  
13 growth medium. Some of the HZE interactions with these target materials may result in  
14 fragmentation of the incident (*i.e.* primary) particle and/or of the target material.  
15 Fragmentation of the incident HZE particle may produce lower-atomic number (Z)  
16 fragments. The primary-particle fragments have a high probability of proceeding with the  
17 same velocity as the primary particle, whereas target fragments generally have lower  
18 velocity and can be scattered with respect to the incident-ion-trajectory (25). Photons and  
19 secondary electrons ( $\delta$  rays), generated as a result of these interactions, can travel,  
20 depending on their energy, significant distances away from the primary particle track  
21 (39).

22 To determine whether secondary particles impart a significant absorbed dose to  
23 either directly targeted cells, or cells in the vicinity, when a mean absorbed dose of

1 0.2 cGy is delivered with either 1000 MeV/u  $^{56}\text{Fe}$  ions, 600 MeV/u  $^{28}\text{Si}$  ions or  
2 290 MeV/u  $^{12}\text{C}$  ions, calculations were undertaken, using FLUKA code version  
3 2011.2.15 (31, 32, 40) with the default configuration ‘HADROTherapy’. FLUKA is a  
4 multi-purpose Monte Carlo particle transport code that considers all particle interactions  
5 including electromagnetic interactions, nuclear interactions of the primary or incident  
6 particles and the generated secondary particles, energy loss fluctuations and Coulomb  
7 scattering.

8 Several parameters were considered in our simulations with FLUKA. They  
9 included transport threshold for particles, delta ray production threshold, and restricted  
10 ionization fluctuations. The RQMD model was used, since its interface was developed for  
11 the processing of ion-ion interactions from 0.1 GeV/u to 5 GeV/u. The event generators  
12 RQMD and DPMJET were linked to ensure ion-ion interactions above 125 MeV/u. The  
13 FLUKA evaporation/fission/fragmentation module performed the fragmentation of the  
14 primary heavy ions and the de-excitation of the excited fragments. Simulations were  
15 undertaken with the transport cut-offs for heavy ions (primary and fragments), photons,  
16 protons and  $\alpha$  particles set at 1 keV. The transport cut-off for electrons was set at 1 keV  
17 when the production threshold for  $\delta$  rays was 10, 100, and 1000 keV; it was set at 150 eV  
18 when the production threshold for  $\delta$  rays was 1 keV. Production thresholds for  $\delta$  rays  
19 were set at equal value in the cover slip, cell monolayer and medium to ensure that the  
20 electronic equilibrium is established (i.e. that the flux of secondary electrons leaving a  
21 surface is independent of the surface thickness). This would be a sensitive parameter for a  
22 very thin surface like the cell monolayer. Upon reaching the cut-off energy, the particles

1 were assumed to deposit this cut-off energy locally and their tracks were no longer  
2 followed.

3 The contribution of neutrons to the absorbed was calculated but is not shown due  
4 to inconsistent results, especially in the cell monolayer. Since the HADROTherapy  
5 option was used, neutrons with energy below 20 MeV cannot be followed with dedicated  
6 multi-group library for neutrons with that energy. Benchmarking the FLUKA code with  
7 the MCNP code could generate more consistent results for the neutron dose.

8 Using FLUKA, the radial dose distribution to the AG1522 cell monolayer around  
9 the track of a narrow beam of 1000 MeV/u  $^{56}\text{Fe}$  ions was calculated for both the primary  
10 particle and its secondaries (HADRONTherapy configuration with delta rays'  
11 production thresholds set at 1, 10, 100, and 1000 keV). Every run was performed with  
12  $10^5$  ions, and the absorbed doses to concentric annuli (thickness 1  $\mu\text{m}$ , depth 1  $\mu\text{m}$ )  
13 extending to a radius of 100  $\mu\text{m}$  were calculated. The radial distance of 100  $\mu\text{m}$  covers  
14 the diameter of an AG1522 cell and extends to adjacent cells.

15 To recreate experimental conditions, the geometry and the constitutive materials  
16 of the flaskettes were introduced into the FLUKA input file. The beam spot at the NSRL  
17 has a uniform center of 20 cm x 20 cm. Within this area, the flaskette containing the cell  
18 monolayer was recreated (Supplementary Figure 1, Panel A). The cell monolayer was  
19 characterized by an area of 10  $\text{cm}^2$  and thickness of 1  $\mu\text{m}$  (i.e. height up to the center of  
20 the nucleus) (41)<sup>1</sup>. The 1 mm-thick soda-lime glass was 19.152  $\text{cm}^2$  in area. The  
21 corresponding volumes were 0.001 and 1.92  $\text{cm}^3$ , respectively, and the volume of the  
22 culture medium was 18.8  $\text{cm}^3$ . The elemental mole percentages of the soda-lime glass

---

<sup>1</sup> The thickness of  $\sim 1 \mu\text{m}$  of an AG1522 cell (41) was estimated from studies in fixed/dehydrated cells grown on Mylar. The actual dimension of a live AG1522 cell grown on glass may be different.

1 (ρ ~2.33 g/cm<sup>3</sup>) were O (60 %), Si (25 %), Na (10 %), Ca (3 %), Mg (1 %) and Al (1 %).  
2 The 1 mm-thick polystyrene (C<sub>8</sub>H<sub>8</sub>) walls of the flaskettes have a density of 1.06 g/cm<sup>3</sup>.  
3 The cell monolayer was assumed to be composed of human skin equivalent (W&W type  
4 3 (42)) with elemental mass composition of H (10.1 %), C (15.8 %), N (3.7 %), O  
5 (69.5 %), S (0.2 %), Cl (0.3 %), Na (0.2 %) and K (0.1 %) and with a density of  
6 1.09 ± 0.05 g/cm<sup>3</sup>. For simplicity, the growth medium was considered to be water with a  
7 thickness of 1.87 cm (flaskette is filled to capacity with culture medium). The flaskette,  
8 thus modeled, was oriented vertically and its growth surface was orthogonal to the  
9 incident beam. The doses calculated by FLUKA were provided as GeV/g cm<sup>3</sup>/primary  
10 ion. Radiation absorbed doses in cGy (Table 2 and Supplementary Tables 2-4) were  
11 obtained from the FLUKA output by correcting the values for target volume and the  
12 fluence. The fluence of 8323 <sup>56</sup>Fe-ions/cm<sup>2</sup> was experimentally determined at BNL by  
13 scintillator-based dosimetry, which relies on counting the tracks in the beam. When a  
14 certain preset number of tracks with high LET characteristic was reached, the beam was  
15 cut-off. This approach was also used in the FLUKA simulations for determining the mean  
16 absorbed dose to the various targets from the primary and secondary radiations.

#### 17 *Western blot analyses*

18 Following irradiation, the cells were harvested by trypsinization, pelleted, rinsed  
19 in PBS, repelleted, and lysed in chilled radio-immune precipitation assay (RIPA) buffer  
20 [50 mM Tris-CI (pH 7.5), 150 mM NaCl, 50 mM NaF, 5 mM EDTA, 1 % (vol/vol)  
21 NP40, 0.5 % (wt/vol) sodium deoxycholate, 0.1 % SDS] supplemented with sodium  
22 orthovanadate (1 mM), and protease (1:1000, vol/vol) and phosphatase (1:1000, vol/vol)

inhibitor cocktails (Sigma). The extracted proteins were fractionated by SDS-PAGE and immunoblotted.

*Protein levels:* Stress responsive proteins were quantified with antibodies against p21<sup>Waf1</sup> (05-345, Millipore), p-TP53ser15 (9284, Cell Signaling), p-ERK1/2 (9101, Cell Signaling) and HDM2 (M4308, Sigma).

*Protein oxidation:* When proteins are oxidized by reactive oxygen species (ROS), some amino acids are modified generating carbonyl groups. These carbonyl groups, specifically of aldehydes or ketones, can react with 2,4-dinitrophenyl hydrazine (DNPH), which may be recognized by anti-2,4 dinitrophenol (DNP) antibodies on immunoblots (43). For experiments, the OxyBlot Protein Oxidation Detection Kit (Millipore) was used. Protein samples were denaturated with 6 % (wt/vol) SDS and derivatized with DNPH. Negative controls were derivatized with a Derivatization-Control solution. After 15 min incubation at room temperature, neutralization solution (2 M Tris/30 % glycerol; vol/vol) was added and samples were immunoblotted. The DNPH-bound proteins were detected with rabbit anti-2,4-dinitrophenyl IgG (Millipore).

*Accumulation of 4-hydroxynonenal adducts:* Hydroxyalkenals, such as 4-hydroxynonenal (4-HNE), are among the major products of lipid peroxidation (44). Proteins with 4-HNE adducts were identified with goat anti-4-HNE antibody (Millipore).

After incubation of the nitrocellulose membranes with a specific secondary antibody conjugated with horseradish peroxidase, protein bands were detected by enhanced chemiluminescence system from GE Healthcare (Amersham). Luminescence was determined by exposure to X ray film, and densitometry analysis was performed with

an EPSON scanner and National Institutes of Health Image J software (NIH Research Services Branch).

Staining of the nitrocellulose membranes with Ponceau S Red (Sigma) was used to verify equal loading of samples (loading control) (45). Experiments were repeated 2 to 7 times, with separate experiments performed to evaluate changes in protein levels, protein oxidation and accumulation of 4-hydroxynonenal adducts. Representative data of immunoblots are shown in Results. Fold changes in the levels of stress responsive proteins in individual experiments together with mean  $\pm$  standard error (SE) are reported in Supplementary Table 1. These changes include the responses of cells targeted by primary ions and those that are not. Treated samples were compared with the control of the respective time point.

#### *In situ immune-detection of 53BP1*

53BP1 is a marker of DNA double-strand breaks (DSB) (46). At different times after irradiation, confluent cells were rinsed twice in PBS, fixed with freshly prepared 3.2 % (vol/vol) paraformaldehyde in PBS for 10 min, and rinsed 5 times with PBS. Subsequently, the cells were permeabilized with Triton-X buffer (0.25 % Triton-X in water / 0.1 % saponin in Tris-buffered saline (TBS) [25 mM Tris, pH 7.5, 150 mM NaCl, 2 mM KCl in water] for 10 min. The fixed and permeabilized cell monolayers were then blocked for 1 h in blocking buffer [2 % (vol/vol) normal goat serum, 2 % (vol/vol) BSA, 0.1 % Triton X-100 (in TBS)] and reacted with rabbit anti-53BP1 antibody (A300-272A, Bethyl) diluted 1:500 (vol/vol) in blocking buffer and incubated for 2 h at room temperature. After incubation with Alexa Fluor 594 goat anti-rabbit secondary antibody (Invitrogen), the cells were washed 3 times (5 min/wash) in buffer consisting of 0.2 %

normal goat serum, 0.2 % BSA, 0.1 % Triton X-100 in TBS. SlowFade® Gold antifade reagent with DAPI (Invitrogen) was used in mounting the samples.

Cells with at least one 53BP1 focus were scored using a UV microscope (Leica DM IL). All the images within the same data set were captured with a ProgRes® camera (Jenoptik) with the same optics and exposure time and were saved for subsequent evaluation. As such, bleaching of the signal was avoided. Identical criteria were followed in defining foci characteristics. Nuclei with atypical size or morphology, and those with very high foci counts (presumably due to replication stress), were not scored (47). The data described in Results represent the excess percent increase of cells with 53BP1 foci in irradiated populations relative to respective control. They were calculated as follows:

$\Delta F = 100 (F_{\text{irradiated}} - F_{\text{control}})$  where F is the ratio of the number of cells with 53BP1 foci over the total number of cells counted.

The results of three independent experiments for energetic iron and silicon ions and  $\alpha$  particles are reported in Results. For each experiment, 2 irradiated and 2 control dishes were analyzed. For each dish, more than 3000 cells were scored by eye in 40 different fields. Poisson statistics was used to calculate the standard error associated with the percentage of cells with foci over the total number of cells scored. The Pearson's  $\chi^2$  test was used to compare treatment groups versus respective controls. A value of  $p \leq 0.05$  between groups was considered significant.

A significant number of cells in control samples harbored foci, which fluctuated between experiments and assay times. When the control samples of all experiments were pooled, the mean  $\pm$  SD of the fraction of cells harboring at least one 53BP1 focus was  $0.26 \pm 0.12$  with a range of 0.05 to 0.50. The mean  $\pm$  SD of spontaneous 53BP1 foci per



cell nucleus was  $0.35 \pm 0.12$  with a range of 0.06 to 0.68 foci/cell. The mean  $\pm$  SD of spontaneous 53BP1 foci per cell nucleus in foci-positive cells was  $1.29 \pm 0.11$  foci/cell with a range from 1.04 to 1.35 foci/cell. These results are consistent with those of Ugenskiene et al. who estimated the background level of 53BP1 foci in AG1522 cells to be 1.1 foci/cell (48). A high background level of nuclear foci indicative of DNA damage was also observed in various cell strains, with inter and intra-individual differences being detected (47).

## RESULTS

### *Significant biological changes are rapidly induced in normal human cell cultures exposed to low fluences of HZE particles*

We investigated stress responses in normal human cell populations exposed to HZE particles under conditions where only a very small fraction of cells is traversed through the nucleus by a primary particle track. To this end, confluent AG1522 cell cultures were exposed to mean absorbed doses of 0.2 or 1 cGy of energetic iron or silicon ions. They were also exposed, in parallel, to  $\alpha$  particles that have been shown to induce significant bystander effects (2, 4, 6, 7). We examined the phosphorylation of serine 15 in TP53 (p-TP53ser15), a marker of DNA damage (49), and of the stress-responsive extracellular signal-related kinases, ERK1 and ERK2 (p-ERK1/2) (50), at different times after irradiation. The observed changes were compared to those in respective controls.

At 15 min after exposure to mean absorbed doses of 0.2 or 1 cGy from 1000 MeV/u  $^{56}\text{Fe}$  ions (LET  $\sim 151$  keV/ $\mu\text{m}$ ) or 600 MeV/u  $^{28}\text{Si}$  (LET  $\sim 50$  keV/ $\mu\text{m}$ ), an increase in p-TP53ser15 and p-ERK1/2 levels was consistently observed (Figure 1, Panel A). Fold-increases of  $1.7 \pm 0.4$  (n=3) and  $2.3 \pm 0.5$  (n=3) in p-TP53ser15 levels,

1 and of  $1.4 \pm 0.1$  (n=3) and  $1.4 \pm 0.1$  (n=3) in p-ERK1/2 levels, were detected in cell  
2 cultures exposed to 0.2 cGy of  $^{56}\text{Fe}$  or  $^{28}\text{Si}$  ions, respectively (representative data shown  
3 in Figure 1, Panel A). At a mean absorbed dose of 0.2 cGy, only ~1.2 and 3.5 % of nuclei  
4 are traversed by either ion, respectively. Similarly, at 1 cGy, wherein ~6 % of nuclei are  
5 traversed by an iron ion and 17.5 % by a silicon ion, respective fold-increases of  $3.2 \pm 1$   
6 (n=6) and  $2.9 \pm 0.5$  (n=4) in p-TP53ser15 levels, and of  $2.7 \pm 0.3$  (n=5) and  $2.4 \pm 0.3$   
7 (n=4) in p-ERK1/2 levels, were observed (representative data shown in Figure 1,  
8 Panel A). Therefore, these data indicate that p-ERK1/2 and p-TP53ser15 are sensitive  
9 markers that are rapidly modulated after exposure of normal human cell cultures to very  
10 low mean absorbed doses of high-LET HZE radiations. The levels of p-TP53ser15 and p-  
11 ERK1/2 were similarly increased at 15 min after exposure of confluent AG1522 cell  
12 cultures to 0.2 cGy ( $1.5 \pm 0.0$  (n=4) and  $1.2 \pm 0.1$  (n=3), respectively) or 1 cGy ( $2.1 \pm 0.3$   
13 (n=7), and  $2.2 \pm 0.2$  (n=6), respectively) of 3.7 MeV  $\alpha$  particles (LET ~109 keV/ $\mu\text{m}$ )  
14 (representative data shown in Figure 1, Panel A). The increase in p-TP53ser15 level,  
15 correlated with increases in the levels of HDM2 and p21<sup>Waf1</sup> at 1 h (Figure 1, Panel B)  
16 and 3 h (Figure 1, Panel C) after irradiation, suggesting activation of TP53, a central  
17 protein involved in maintenance of genomic integrity. Similar increases in TP53  
18 signaling were also observed at 6 and 24 h after irradiation (Figure 1, Panel D). For all  
19 treatments, the results of individual experiments are described in supplementary Table 1.

20 Likewise,  $3.3 \pm 1.4$  (n=3) and  $6.5 \pm 1.8$  (n=3)-fold increases in overall protein  
21 carbonylation were detected in extracts of cell cultures harvested 24 h after exposure to  
22 0.2 and 1 cGy of 1000 MeV/u iron ions, respectively (representative data in Figure 2,  
23 Panel A). The accumulation of 4-hydroxynonenal (HNE) adducts in proteins from the

1 same cultures indicates that increased lipid peroxidation was involved (representative  
2 data in Figure 2, Panel B). A  $1.8 \pm 0.2$  (n=3) and  $3.8 \pm 1.4$  (n=3) fold increases in  
3 proteins with 4-HNE adducts were detected at 24 h after exposure to 0.2 and 1 cGy of  
4 1000 MeV/u iron ions, respectively.

5       The induction of stressful effects and their persistence, in low fluence-irradiated  
6 cell cultures, was further revealed when confluent cultures exposed to 1 cGy from  
7 1000 MeV/u  $^{56}\text{Fe}$  ions were subcultured to lower density (1:3) in fresh medium within  
8 15 min after irradiation. Relative to control, increases in the levels of p-TP53ser15,  
9 p21<sup>Waf1</sup> and HDM2 occurred at 8 and 24 h after subculture (Figure 3). Together, the  
10 magnitude of the various changes, in confluent and growing cell populations, suggests  
11 participation of a greater proportion of cells in the stress response than the 1.2-3.5 %  
12 fraction traversed by a primary particle track through the nucleus at a mean dose of  
13 0.2 cGy. For example, for the  $3.2 \pm 1.0$  (n=6)-fold-increases in p-TP53ser15 detected at  
14 15 min, and  $2.5 \pm 0.3$  fold (n=5)-increases in p21<sup>Waf1</sup> levels detected at 3 h after exposure  
15 of cell cultures to 1 cGy of  $^{56}\text{Fe}$  ions, to be solely due to effects in cells targeted through  
16 the nucleus by a primary ion, the cells would have to increase the level of these stress-  
17 responsive proteins by ~50-folds.

#### 18 *53BP1 foci formation in AG1522 cell cultures exposed to low fluences of HZE particles*

19       To evaluate stressful effects in confluent cultures exposed to low fluences of  
20 HZE-particles on a cell by cell basis, we examined 53BP1 foci formation *in situ* at  
21 15 min, 1 h, 3 h and 24 h after exposure to 0.2 cGy of either 1000 MeV/u  $^{56}\text{Fe}$  ions,  
22 600 MeV/u  $^{28}\text{Si}$  ions or 3.7 MeV  $\alpha$  particles. Separate cell cultures that received no  
23 radiation, but were sham-treated, were included for each time point and were considered

as respective controls (Figure 4). Whereas, only ~1.2-3.5 % of the cell nuclei are traversed by a primary HZE particle (Table 1), relative to respective control, the percent of cells with 53BP1 foci was increased at 15 min, 1 h and 3 h by 6.8 % ( $p < 0.001$ ), 15 % ( $p < 0.001$ ) and 10.6 % ( $p < 0.001$ ), respectively for  $^{56}\text{Fe}$  ions (Figure 4, Panel A, experiment #1), and by 1.9 %, 7.7 % ( $p < 0.001$ ), and 5.3 % ( $p < 0.001$ ), respectively, for 3.7 MeV  $\alpha$  particles (Figure 4, Panel B, experiment #1). Increases of 8.2 % ( $p < 0.001$ ), 11.4 % ( $p < 0.001$ ) and 2.8 % ( $p < 0.05$ ), at 15 min, 1 h and 3 h, respectively, were also observed after exposure to 0.2 cGy of  $^{28}\text{Si}$  ions (Figure 4, Panel C, experiment #1). By 24 h, the percent increase of cells with 53BP1 foci was null for  $^{56}\text{Fe}$  ions, was increased by 3.1 % ( $p < 0.01$ ) for  $^{28}\text{Si}$  ions, and by 2 % for  $\alpha$  particles ( $p < 0.05$ ). The significant increases in the excess percent of cells with foci (1.9–15 %) over what would be expected based on the percentage of cells irradiated through the nucleus (1.2-3.5 %) strongly support the participation of cells that were not targeted by the primary particle in the overall response of the cell population to irradiation by low fluences of high LET particles. Although the magnitude of the response varied between experiments, the trend was similar. At 1 h following irradiation by a mean absorbed dose of 0.2 cGy from iron ions, the increases in 53BP1 foci observed in experiments 2 and 3 were 10.3 % ( $p < 0.001$ ) and 7.3 % ( $p < 0.001$ ), respectively, compared to 15 % ( $p < 0.001$ ) in experiment 1 (Figure 4).

The fraction of cells with foci was shown to decrease by 2 h after exposure to DNA damaging agents (23). Thus, the increases observed at 1-3 h over those detected at 15 min in cultures exposed to  $^{56}\text{Fe}$  ions or  $\alpha$  particles could be due to recruitment of additional cells in the response. Presumably, these are bystander cells wherein signaling

1 molecules propagated from irradiated cells had time to exert effects that result in DNA  
2 damage. Whereas the attenuation of the percent increase of cells with 53BP1 foci at 24 h  
3 in iron ion- and  $\alpha$ -particle-irradiated cells and at 3-24 h in silicon ion-irradiated cells may  
4 reflect repair of DNA damage in bystander cells, the persistent foci detected at these later  
5 times presumably reside in cells that were directly targeted by densely ionizing particles.

6 In contrast to  $^{56}\text{Fe}$  ions (LET  $\sim 151$  keV/ $\mu\text{m}$ ),  $^{28}\text{Si}$  ions (LET  $\sim 50$  keV/ $\mu\text{m}$ ) and  
7  $\alpha$  particles (LET  $\sim 109$  keV/ $\mu\text{m}$ ), exposure of confluent cultures to 0.2 cGy from  
8 290 MeV/u  $^{12}\text{C}$  ions (LET  $\sim 13$  keV/ $\mu\text{m}$ ) did not result in significant increase in the  
9 percentage of cells with 53BP1 foci (not shown). This suggests that low mean absorbed  
10 doses of HZE particles with lower LET may be less efficient at inducing stressful effects  
11 (i.e. 53BP1 foci) under the conditions used in this study.

#### 12 *Cell culture system to identify cells irradiated with an HZE particle*

13 Solid-state track detectors fused to cell culture dishes can be used to identify the  
14 position of primary HZE particle traversals. Experiments performed with such dishes  
15 suggested that the induction of stress in the form of 53BP1 foci is also observed in cells  
16 not traversed by primary HZE particles. We bonded a 100  $\mu\text{m}$ -thick PADC solid state  
17 nuclear track detector (SSNTD) to the bottom edges of the cell culture surface  
18 (Supplementary Figure 1, Panel B). After etching of PADC plastic, cells that were likely  
19 traversed by a particle track could be identified, and induced biological effects may be  
20 assessed by suitable markers. The data in Figure 5 show 53BP1 foci in a confluent cell  
21 culture exposed to 0.2 cGy of 1000 MeV/u  $^{56}\text{Fe}$  ions followed by 15 min incubation.  
22 Following cell fixation and etching of PADC, the iron ion tracks were visible as black  
23 dots (Figure 5, Panel A). Exposure to 0.2 cGy generally resulted in  $\sim 1.5$  % of cells'

nuclei being superimposed on pits. The formation of 53BP1 foci (Figure 5, Panel B) in nuclei (revealed by DAPI staining, Figure 5, Panel C) that superimpose the black dots (inverted in white for better visualization, Figure 5, Panel D) indicates that these cells sustained DNA damage as would be expected from nuclear traversal by a high LET particle. The two cells with foci adjacent to the traversed cell are likely affected cells that were not targeted by the primary particle (Figure 5, Panel D). They may be bystander cells or cells subject to secondary radiations. The absence of SSNTD pits below these adjacent cells indicates lack of hot-spots; it suggests that the strategy of incorporating solid state nuclear track detector would be suitable for investigating the kinetics of biologic responses *in situ* in targeted and non-targeted cells.

*The significance of secondary radiations in biological responses of cell cultures exposed to low fluence HZE particles*

Secondary radiations resulting from the interaction of primary HZE particles with the target materials may have had a role in the apparent bystander effects. To shed additional light on this possibility, the contribution of secondary particles to the mean absorbed dose was calculated by simulations using the FLUKA multi-particle transport code (Table 2 and supplementary Tables 2-4). Estimates of the doses from heavy ions (primary and fragments), electrons, photons, protons and  $\alpha$  particles to the AG1522 *cell monolayer* following exposure to a mean absorbed dose of 0.2 cGy from 1000 MeV/u  $^{56}\text{Fe}$  ions, 600 MeV/u  $^{28}\text{Si}$  ions or 290 MeV/u  $^{12}\text{C}$  ions are described in Table 2. When exposed to any of the primary ions, secondary radiations consisting of HZE fragments, photons, protons and  $\alpha$  particles, with a production threshold and a transport cut-off set at 1 keV, constituted <1 % of the total absorbed dose (Table 2). In contrast, electrons with a

1 production threshold set at 1 keV and transport cut-off set at 150 eV contributed ~37-  
2 40 % of the total dose. The mean absorbed dose deposited in the cell monolayer by  
3 HZE fragments was very small (0.0007 cGy, 0.0004 cGy and 0.0005 cGy following  
4 exposure to  $^{56}\text{Fe}$  ions,  $^{28}\text{Si}$  ions or  $^{12}\text{C}$  ions, respectively) (Table 2). The dose contributed  
5 by photons, protons and  $\alpha$  particles was minimal in all cases (Table 2).

6 Estimates of the mean absorbed doses to the glass cover-slip, cell monolayer and  
7 growth medium due to secondary radiations when the production threshold of  $\delta$  rays was  
8 set at 1, 10 100 or 1000 keV and the transport cut off was set at 1 keV are described in  
9 Supplementary Tables 2-4. As the production threshold of the  $\delta$  rays increased, the  
10 contribution of secondary electrons to the total mean absorbed dose delivered to the *cell*  
11 *monolayers* decreased and that of primary ions increased. Specifically, when the  $\delta$  rays'  
12 production threshold was set at 1000 keV, the contribution of primary ions to the total  
13 mean absorbed dose to a *cell monolayer* exposed to 1000 MeV/u  $^{56}\text{Fe}$  ions increased to  
14 ~97 % and that of electrons decreased to ~2 % (supplementary Table 2). In case of  
15 600 MeV/u  $^{28}\text{Si}$  ions and 290 MeV/u  $^{12}\text{C}$  ions, the secondary electrons represented,  
16 respectively, 0.96 % and almost nil of the total mean absorbed dose to the *cell monolayer*  
17 (Supplementary Tables 3 and 4).

18 Quantifying the radial distribution of the secondary particles is essential before  
19 attributing stressful effects, observed in cells that surround directly targeted cells to a  
20 bystander effect. The data in Figure 6 represent the radial dose distributions (heavy ions,  
21 electrons and the total dose) in a 1  $\mu\text{m}$ -thick cell culture layer exposed to an orthogonal  
22 narrow beam of 1000 MeV/u  $^{56}\text{Fe}$  ions. Panel A shows that the heavy ions deposit their  
23 energy mainly in the first 10  $\mu\text{m}$ , while the electron dose extends out to ~100  $\mu\text{m}$  radius

1 around the track of the primary ion. Panel B describes the radial distribution of dose from  
2  $\delta$  rays with 1-, 10-, 100 or 1000 keV-production-thresholds. Panels C and D permit  
3 visualization of the radial dose deposited by heavy ions or electrons, respectively, around  
4 the primary track pit revealed by etching of PADC and staining nuclei with DAPI as  
5 described in Figure 5 (Panel D). It is noteworthy that the magnitude of the total radial  
6 dose distribution, calculated in our studies, is in accord with previous results (51).

7 In the FLUKA code, the ionization energy losses are processed as continuous  
8 energy loss or as discrete ionization events. Above the pre-set threshold, the ionization is  
9 modeled as production of  $\delta$  rays, based on scattering of the projectile with a free electron.  
10 This threshold of  $\delta$  ray production is an important parameter in this type of simulation. At  
11 radial distances less than 20  $\mu\text{m}$  from the track, the calculated absorbed dose depends  
12 strongly on the threshold value (1, 10 or 100 keV) (Figure 6, Panel B). As expected, low  
13 thresholds should be used to accurately simulate radial dose distributions around the track  
14 core with  $\mu\text{m}$  and sub- $\mu\text{m}$  spatial resolution (52).

15 The data in Figure 6 therefore imply that, in our experiments, the chance for  
16 heavy fragments to hit neighboring cells is negligible. However, this is not the case for  
17 secondary electrons which can travel significant distances from the track. Energy  
18 deposition by  $\delta$  rays is a stochastic process, and the possibility exists that some cells in  
19 the vicinity of cells targeted by a primary ion may receive a biologically relevant dose.

## 20 DISCUSSION

21 The lack of clear knowledge about non-targeted responses has been singled out by  
22 the US National Academies (53) as one of the important factors limiting the prediction of  
23 radiation health risks associated with space exploration. During deep space missions,



1 every cell nucleus in an astronaut's body would be hit by a proton or secondary electron  
2 every few days and by an HZE ion about once a month (54); the rest would be  
3 bystanders. Human epidemiological studies would be ideal to predict the health risks of  
4 exposure to low fluences of space particulate radiations; however, given the relatively  
5 insignificant number of humans exposed to such radiations, mechanistic studies in cell  
6 culture systems and animals are critical to help estimate corresponding risks to humans.

7       Using molecular, biochemical, physical and computational approaches, here we  
8 provide evidence for the amplification of HZE-particle-induced stressful effects in  
9 normal human fibroblast cultures following exposure to doses as low as 0.2 cGy of  
10 1000 MeV/u iron ions or 600 MeV/u silicon ions (Figures 1-5). Consistent with previous  
11 results in cell cultures exposed to low fluences of  $\alpha$  particles, another type of radiation  
12 with similar quality (i.e. high LET character), increases in the levels of proteins that  
13 participate in TP53 and ERK1/2 signaling pathways (55) were observed. These increases  
14 were detected as early as 15 min after irradiation and persisted for at least 24 h. Relative  
15 to control, higher levels of p-TP53ser15, a marker of DNA damage, was detected in  
16 confluent AG1522 fibroblasts exposed to a mean absorbed dose of 0.2 cGy that targets,  
17 on average, only 1-3 % of the cells through the nucleus. This was associated 1-3 h later  
18 (Figure 1, Panels B and C) with increased level of p21<sup>Waf1</sup>, a p53 effector and key  
19 component of the DNA damage induced G<sub>1</sub> checkpoint. The induction of these stress  
20 markers persisted for at least 24 h (Figure 1, Panel D) and was associated with an  
21 increase in protein carbonylation and in accumulation of 4-HNE protein adducts  
22 (Figure 2, Panels A and B). Interestingly, 4-HNE reactive aldehydes originate from  
23 peroxidation of membrane lipids where key proteins that mediate stress-induced

bystander effects, including connexins, cyclooxygenase-2 and NAD(P)H oxidase, reside (56). The accumulation of such protein adducts may modulate transport properties of the plasma membrane, gene expression, including signal transduction pathways affecting DNA damage sensing and repair, cell survival and cell proliferation (57). The occurrence of such appreciable oxidative effects, long after exposure, is consistent with excess ROS generation due to perturbations in oxidative metabolism and/or persistent activation of oxidases (58, 59). It suggests the involvement of a greater fraction of cells than those targeted by a primary particle in the overall response leading to oxidative stress. Whereas the persistence of stress may be due to sustained changes in the targeted and non-targeted cells that were affected early after exposure, it could also result from induction of stress in additionally recruited cells that were not-targeted by a primary particle. This does not preclude, however, the restitution of damage and return to the basal state in certain affected non-targeted and targeted cells.

The DNA DSB is a serious threat to the integrity of eukaryotic genomes (60). Following exposure to DNA damaging agents, a battery of damage sensing and repair proteins localize at the site of DNA breaks. Among these proteins, 53BP1 forms discrete foci within minutes after exposure (23, 46, 61). Here, we used the formation of 53BP1 foci as a biomarker to investigate the evolution of  $\alpha$ - and HZE-particle-induced propagation of signaling events leading to DNA damage in cells that were not targeted by a primary particle. We used the same microscope optics and exposure time, and scored by eye to accurately differentiate foci; we also used separate controls for each time point. Utilizing these criteria, the results from cultures exposed to a dose by which only 1-3 % of cells are traversed through the nucleus by a primary energetic ion strongly supported

1 the participation of cells other than those targeted by the primary particles in the  
2 response. At 15 min after exposure to 0.2 cGy from  $\alpha$  particles,  $^{56}\text{Fe}$  ions or  $^{28}\text{Si}$  ions, the  
3 fraction of cells with 53BP1 foci was higher than predicted based on the percentage of  
4 nuclei directly targeted by primary ions (Figure 4). Whereas secondary radiation may  
5 have contributed to the effects observed in the HZE-particle irradiated cell cultures, this  
6 cannot be the case in the studies using our  $\alpha$  particle irradiator. The ranges of  $\delta$  rays  
7 produced by the interaction of these  $\alpha$  particles (3.7 MeV, 0.5 MeV FWHM) with the  
8 cells are very small compared with the nuclear diameter. Hence, the effects observed in  
9  $\alpha$ -particle-irradiated cell cultures (Figure 4) clearly support the spread of stressful effects  
10 to unirradiated bystander cells.

11 In general, it is thought that 53BP1 foci formation is transient. Following uniform  
12 exposure of cell cultures to an absorbed dose of 1 Gy from  $^{137}\text{Cs}$   $\gamma$  rays, the fraction of  
13 cells with foci peaked at 20 min and remained elevated for 2 h after irradiation; it  
14 decreased exponentially and returned to basal level 16 h later (23). In our study with cell  
15 cultures where only 1.2-3.5 % of nuclei were irradiated with  $\alpha$  particles, iron ions or  
16 silicon ions, the maximum increase in the fraction of cells with 53BP1 foci was detected  
17 at 1 h. The persistent elevation in foci formation at 3 h may be due to the induction of  
18 DNA damage in non-directly targeted cells. At 3 h after exposure, foci formation in iron  
19 ion- and  $\alpha$ -particle-irradiated cultures was increased not only over control but also  
20 compared to cultures examined at 15 min after irradiation ( $p < 0.001$ ). Whereas, the  
21 increases in the fraction of cells with foci at 1 and 3 h may reflect the spread of stressful  
22 effects to additional cells than those targeted by radiation, they may also reflect

development of foci in affected cells (irradiated and bystander) that required time to become visible by microscopy.

In contrast to  $^{56}\text{Fe}$  ions,  $^{28}\text{Si}$  ions and  $\alpha$  particles, no excess 53BP1 foci formation has been detected after exposure of cell cultures to 0.2 cGy from 290 MeV/u carbon ions (LET  $\sim 13$  keV/ $\mu\text{m}$ ) at any time between 15 min and 24 h after irradiation. This may be due to less complex DNA damage being induced in the targeted cells, which may affect the nature of the propagated signaling events. At a mean absorbed dose of 0.2 cGy to the exposed cultures from 290 MeV/u carbon ions,  $\sim 0.015$  cGy are deposited in the nucleus from a single particle traversal; in comparison,  $\sim 17.25$  cGy, 5.7 cGy and 12.45 cGy are deposited by single traversals of 1000 MeV/u Fe, 600 MeV/u silicon and 3.7 MeV  $\alpha$  particles<sup>2</sup>, respectively. Thus, the dose absorbed by the targeted nuclei likely plays an important role in the induction of stressful effects leading to DNA damage. Different targeted and non-targeted effects may however occur following cellular hits with multiple carbon ions. The use of microbeams would greatly facilitate such experiments and would be informative of the effects of absorbed dose and radiation quality.

Culture dishes that incorporate nuclear track etch detectors were developed in order to identify cells and cell nuclei traversed by primary HZE particles. Our preliminary experiments suggest that the induction of stress in the form of 53BP1 foci is also observed in cells that were not traversed by a primary  $^{56}\text{Fe}$  ion. The strategy of using culture dishes with nuclear track detector to examine biological changes in HZE-particle-irradiated cultures expanded our previous studies with  $\alpha$  particles (34), and permitted irradiation of cell cultures grown in dishes with sealable-lid in presence of pH-

---

<sup>2</sup> The absorbed dose ( $d$ ) per traversal to the thin disk-shaped cell nucleus of the AG1522 cell was calculated according to the relation  $d = (0.16 \text{ LET})/(A \rho)$ , where  $A$  is the cross-sectional area of the cell nucleus (i.e. an average of  $\sim 140 \mu\text{m}^2$ ), and  $\rho$  is the density of the cell.

1 equilibrated culture medium with a horizontal broadbeam. Time-course experiments  
2 using these dishes, together with determination of the metrology of distance propagation  
3 as we have previously done with low fluence  $\alpha$ -particle-irradiated cell cultures (34),  
4 would be highly informative of the kinetics of induction and decay of biological changes  
5 in cell cultures exposed to low fluences of HZE particle. In such studies careful  
6 characterization of the positional accuracy of the primary track is essential. A typical  
7 10  $\mu\text{m}$  spatial deviation may have to be considered due to scattering of the incident ion as  
8 it crosses the polymer material of the nuclear track etch detector.

9       To evaluate the possibility of whether the stressful effects expressed in presumed  
10 bystander cells in low fluence HZE-particle-irradiated cultures may be due to secondary  
11 particles generated from fragmentation of the incident beam in the target material  
12 (Table 2, Supplementary Tables 2-4), we performed computational simulations using the  
13 FLUKA multi-particle transport code. The capabilities of this code have been  
14 demonstrated in simulations for microdosimetric purposes and tissue equivalent  
15 proportional counters (51, 62). Our simulations showed that, using glass-bottomed  
16 flaskettes, the total dose to the monolayer due to HZE fragments is negligible.  
17 Importantly, the radial dose due to these fragments is confined to  $\sim 10\ \mu\text{m}$  around the  
18 primary track. In contrast, the dose due to  $\delta$  rays may be substantial. Depending on  
19 energy, the range of the  $\delta$  rays can be extensive (e.g.,  $\sim 130\ \mu\text{m}$  for 100 keV  $\delta$  rays) (63,  
20 64), thus likely targeting all cells in the exposed culture (Figure 6). Whereas, the  
21 biological effects induced by  $\delta$  rays may be stressful, they can also attenuate damaging  
22 effects propagated from cells targeted with primary and HZE fragments. In case of cells  
23 exposed to 3.7 MeV  $\alpha$  particles, the complications in interpreting the apparent bystander

1 effects (Figures 1 and 4) are diminished, as these particles do not produce secondary  
2 radiation that cross-irradiate neighboring cells (26).

3 Experimental systems that allow deciphering the nature of biological effects due  
4 to  $\delta$  rays and to the primary HZE fragments would be highly informative towards  
5 understanding the spectrum of biological changes induced following exposure to low  
6 fluences of HZE particles. In this context, co-culture systems that allow investigation of  
7 HZE-particle-induced non-targeted effects in the absence of secondary fragmentation  
8 products, or  $\delta$  rays, generated strong evidence for the propagation from irradiated cells of  
9 signaling events leading to oxidative stress and DNA damage in bystander cells, an effect  
10 that persisted in their progeny (18). Importantly, the expansion of HZE-particle-induced  
11 non-targeted effects to *in vivo* systems (65), together with characterization of the  
12 magnitude of effects due to fragmentation products, the modulating effect of  $\delta$  rays, and  
13 of the underlying mechanisms, is of importance to human space exploration and hadron  
14 therapy (66). In particular, exposure of biological specimens at very low dose-rate to  
15 simulate more closely the doses received during space travel (54) would be essential.  
16 During a 24 h period, these doses are significantly lower than the lowest dose of 0.2 cGy  
17 used in our studies.

## 18 CONCLUSION

19 The data reported here highlight the manifestation of stressful effects in confluent  
20 normal human cell cultures exposed to low fluences of HZE particles by several  
21 endpoints. The results show that propagation of the signaling events leading to stressful  
22 effects in cells not targeted by a primary particle is rapid, but the reaction to the  
23 propagated signal(s) may require time to be expressed depending on the endpoint

1 investigated. The phenotype (e.g. redox environment) of both, the signal emitting cells  
2 and the recipient cells may greatly affect the kinetics of expression of biological changes.  
3 Indeed, studies have shown that the DNA repair capacity of non-targeted cells (67, 68),  
4 their anti-oxidant potential (69), and their genotype (70) modulate bystander effects. The  
5 results with 53BP1 foci formation showed that by 24 h after exposure to 1000 MeV/u  
6  $^{56}\text{Fe}$  ions, the excess formation of foci was greatly reduced. This may suggest that the  
7 induction of DNA damage in presumed bystander cells is transient; however,  
8 accumulating data from experiments involving co-cultures of HZE-particle-irradiated  
9 cells with unirradiated bystander cells show that the latter experience genomic instability  
10 that manifests in perturbations in oxidative metabolism (18) and excess chromosomal  
11 damage in their progeny (11, 19).

12 Additional FLUKA calculations to determine both the fraction of cells that were  
13 not targeted by fragmentation products and the fraction of cells that were hit by these  
14 products together with the doses received are necessary to enhance our understanding of  
15 low fluences HZE particle- induced bystander effects. This approach will require a  
16 different model, with individual cells being considered under the same experimental  
17 conditions. Depending on cell culture conditions (e.g. glass versus polystyrene platform  
18 for cell growth, thickness of platform, cell thickness etc.) the yield and nature of  
19 fragmentation products may vary, which may impact the signaling pathways leading to  
20 enhancement or attenuation of stressful effects expressed in the exposed cell cultures.  
21 The physical and physico-chemical events resulting from irradiation with primary or  
22 secondary fragments (71-73), including yield, lifetime and spatial distribution of the  
23 generated radiolytic species may induce prominent biochemical and genetic changes that

1 affect intercellular communication between irradiated and bystander cells, which may  
2 modulate the magnitude of the induced stress response and determine long-term  
3 biological effects. Together, these studies may greatly contribute to the efforts by NASA  
4 to develop risk based radiation exposure guidelines that minimize adverse health effects  
5 in astronauts.

## 6 **ACKNOWLEDGMENTS**

7 We thank Dr. Peter Guida and his team at the NASA Space Radiation Laboratory  
8 for their support during the experiments. We are grateful to Drs. Adam Rusek, Michael  
9 Sivertz and I-Hung Chang for dosimetry support. We thank Drs. Hatsumi Nagasawa, Les  
10 Braby and John Ford for their gift of polyethylene terephthalate. We also thank Gary  
11 Moss from Track Analysis Systems Ltd. for his input in developing the dishes with  
12 Tastrak™-bottom. The input of Manuela Buonanno, Narongchai Autsavapornporn and  
13 Jie Zhang in the course of the experiments is greatly appreciated. This research was  
14 supported by NASA Grant NNJ06HD91G and by Grant CA049062 from the National  
15 Institute of Health; RWH is supported by grant CA83838 from the National Institute of  
16 Health.

## 17 **REFERENCES**

- 18 1. Little JB. Genomic instability and bystander effects: a historical perspective.  
19 Oncogene 2003; 22:6978-87.
- 20 2. Nagasawa H, Little JB. Induction of sister chromatid exchanges by extremely low  
21 doses of  $\alpha$ -particles. Cancer Res 1992; 52:6394-6.



- 1 3. Nagasawa H, Little JB. Unexpected sensitivity to the induction of mutations by  
2 very low doses of alpha-particle irradiation: Evidence for a bystander effect.  
3 Radiat Res 1999; 152:552-7.
- 4 4. Zhou H, Randers-Pehrson G, Waldren CA, Vannais D, Hall EJ, Hei TK.  
5 Induction of a bystander mutagenic effect of alpha particles in mammalian cells.  
6 Proc Natl Acad Sci USA 2000; 97:2099-104.
- 7 5. Ponnaiya B, Jenkins-Baker G, Bigelow A, Marino S, Geard CR. Detection of  
8 chromosomal instability in alpha-irradiated and bystander human fibroblasts.  
9 Mutat Res 2004; 568:41-8.
- 10 6. Azzam EI, de Toledo SM, Little JB. Direct evidence for the participation of gap-  
11 junction mediated intercellular communication in the transmission of damage  
12 signals from alpha-particle irradiated to non-irradiated cells. Proc Natl Acad Sci  
13 USA 2001; 98:473-8.
- 14 7. Azzam EI, de Toledo SM, Gooding T, Little JB. Intercellular communication is  
15 involved in the bystander regulation of gene expression in human cells exposed to  
16 very low fluences of alpha particles. Radiat Res 1998; 150:497-504.
- 17 8. Hickman AW, Jaramillo RJ, Lechner JF, Johnson NF. Alpha-particle-induced p53  
18 protein expression in a rat lung epithelial cell strain. Cancer Res 1994; 54:5797-  
19 800.
- 20 9. Sowa MB, Goetz W, Baulch JE, Pyles DN, Dziegielewska J, Yovino S, et al. Lack  
21 of evidence for low-LET radiation induced bystander response in normal human  
22 fibroblasts and colon carcinoma cells. Int J Radiat Biol 2010; 86:102-13.

- 1 10. Sawant SG, Randers-Pehrson G, Geard CR, Brenner DJ, Hall EJ. The bystander  
2 effect in radiation oncogenesis: I. Transformation in C3H 10T1/2 cells in vitro  
3 can be initiated in the unirradiated neighbors of irradiated cells. Radiat Res 2001;  
4 155:397-401.
- 5 11. Buonanno M, de Toledo SM, Azzam EI. Increased frequency of spontaneous  
6 neoplastic transformation in progeny of bystander cells from cultures exposed to  
7 densely-ionizing radiation. PloS one 2011; 6: art. no. e21540.
- 8 12. Shao C, Furusawa Y, Kobayashi Y, Funayama T, Wada S. Bystander effect  
9 induced by counted high-LET particles in confluent human fibroblasts: a  
10 mechanistic study. FASEB J 2003; 17:1422-7.
- 11 13. Hamada N, Ni M, Funayama T, Sakashita T, Kobayashi Y. Temporally distinct  
12 response of irradiated normal human fibroblasts and their bystander cells to  
13 energetic heavy ions. Mutat Res 2008; 639:35-44.
- 14 14. Harada K, Nonaka T, Hamada N, Sakurai H, Hasegawa M, Funayama T, et al.  
15 Heavy-ion-induced bystander killing of human lung cancer cells: role of gap  
16 junctional intercellular communication. Cancer Sci 2009; 100:684-8.
- 17 15. Fournier C, Becker D, Winter M, Barberet P, Heiss M, Fischer B, et al. Cell  
18 cycle-related bystander responses are not increased with LET after heavy-ion  
19 irradiation. Radiat Res 2007; 167:194-206.
- 20 16. Yang H, Anzenberg V, Held KD. The time dependence of bystander responses  
21 induced by iron-ion radiation in normal human skin fibroblasts. Radiat Res 2007;  
22 168:292-8.

- 1 17. Yang H, Anzenberg V, Held KD. Effects of heavy ions and energetic protons on  
2 normal human fibroblasts. Radiatsionnaia biologii, radioecologii / Rossiiskaia  
3 akademiia nauk 2007; 47:302-6.
- 4 18. Buonanno M, De Toledo SM, Pain D, Azzam EI. Long-term consequences of  
5 radiation-induced bystander effects depend on radiation quality and dose and  
6 correlate with oxidative stress. Radiat Res 2011; 175:405-15.
- 7 19. Ponnaiya B, Suzuki M, Tsuruoka C, Uchihori Y, Wei Y, Hei TK. Detection of  
8 chromosomal instability in bystander cells after Si490-ion irradiation. Radiat Res  
9 2011; 176:280-90.
- 10 20. Groesser T, Cooper B, Rydberg B. Lack of bystander effects from high-LET  
11 radiation for early cytogenetic end points. Radiat Res 2008; 170:794-802.
- 12 21. Fournier C, Barberet P, Pouthier T, Ritter S, Fischer B, Voss KO, et al. No  
13 evidence for DNA and early cytogenetic damage in bystander cells after heavy-  
14 ion microirradiation at two facilities. Radiat Res 2009; 171:530-40.
- 15 22. Cucinotta FA, Chappell LJ. Non-targeted effects and the dose response for heavy  
16 ion tumor induction. Mutat Res 2010; 687:49-53.
- 17 23. Schultz LB, Chehab NH, Malikzay A, Halazonetis TD. p53 binding protein 1  
18 (53BP1) is an early participant in the cellular response to DNA double-strand  
19 breaks. J Cell Biol 2000; 151:1381-90.
- 20 24. Goodhead DT. The initial physical damage produced by ionizing radiations. Int J  
21 Radiat Biol 1989; 56:623-34.
- 22 25. Ponomarev AL, Cucinotta FA. Nuclear fragmentation and the number of particle  
23 tracks in tissue. Radiat Prot Dosimetry 2006; 122:354-61.

- 1 26. Hamm RN, Turner JE, Ritchie RH, Wright HA. Calculation of heavy-ion tracks in  
2 liquid water. Radiat Res 1985; 104:S20-S6.
- 3 27. Cucinotta F, Nikjoo H, Goodhead DT. The effect of delta rays on the number of  
4 particle traversals per cell in laboratory and space exposures. Radiat Res 1998;  
5 150:115-19.
- 6 28. Metting NF, Rossi HH, Braby LA, Kliauga PJ, Howard J, Zaider M, et al.  
7 Microdosimetry near the trajectory of high-energy heavy ions. Radiat Res 1988;  
8 116:183-95.
- 9 29. Elmore E, Lao XY, Kapadia R, Redpath JL. Threshold-type dose response for  
10 induction of neoplastic transformation by 1 GeV/nucleon iron ions. Radiat Res  
11 2009; 171:764-70.
- 12 30. Aiginger H, Andersen V, Ballarini F, Battistoni G, Campanella M, Carboni M, et  
13 al. The FLUKA code: new developments and application to 1 GeV/n iron beams.  
14 Adv Space Res 2005; 35:214-22.
- 15 31. Battistoni G, Muraro S, Sala PR, Cerutti F, Ferrari A, Roesler S, et al., The  
16 FLUKA code: Description and benchmarking. In *Proceedings of the Hadronic*  
17 *Shower Simulation Workshop 2006* (A. Albrow RR, Ed.), pp. 31-49. AIP  
18 Conference Proceeding, Fermilab, 2007.
- 19 32. FLUKA: A Multi-Particle Transport Code. Geneva: CERN European  
20 organization for nuclear research; 2005.
- 21 33. Terasima T, Tolmach LJ. Changes in x-ray sensitivity of HeLa cells during the  
22 division cycle. Nature 1961; 190:1210-11.

- 1 34. Gaillard S, Pusset D, de Toledo SM, Fromm M, Azzam EI. Propagation distance  
2 of the alpha-particle-induced bystander effect: the role of nuclear traversal and  
3 gap junction communication. *Radiat Res* 2009; 171:513-20.
- 4 35. Gray LH, Conger AD, Ebert M, Hornsey S, Scott OC. The concentration of  
5 oxygen dissolved in tissues at the time of irradiation as a factor in radiotherapy.  
6 *Br J Radiol* 1953; 26:638-48.
- 7 36. Rueckert RR, Mueller GC. Effect of oxygen tension on HeLa cell growth. *Cancer*  
8 *Res* 1960; 20:944-9.
- 9 37. Neti PV, de Toledo SM, Perumal V, Azzam EI, Howell RW. A multi-port low-  
10 fluence alpha-particle irradiator: fabrication, testing and benchmark  
11 radiobiological studies. *Radiat Res* 2004; 161:732-8.
- 12 38. Charlton DE, Sephton R. A relationship between microdosimetric spectra and cell  
13 survival for high-LET irradiation. *Int J Radiat Biol* 1991; 59:447-57.
- 14 39. Cucinotta FA, Katz R, Wilson JW. Radial distribution of electron spectra from  
15 high-energy ions. *Radiat Environ Biophys* 1998; 37:259-65.
- 16 40. FLUKA. Version 2011.2.12. Battistoni G, Broggi F, Brugger M, Campanella M,  
17 Carboni M, Empl A, et al. 2011.
- 18 41. Cornforth MN, Schillaci ME, Goodhead DT, Carpenter SG, Wilder ME, Sebring  
19 RJ, et al. Radiobiology of ultrasoft X rays. III. Normal human fibroblasts and the  
20 significance of terminal track structure in cell inactivation. *Radiat Res* 1989;  
21 119:511-22.
- 22 42. Woodard HQ, White DR. The composition of body tissues. *Br J Radiol* 1986;  
23 59:1209-18.

- 1 43. Stadtman ER. Oxidation of free amino acids and amino acid residues in proteins  
2 by radiolysis and by metal-catalyzed reactions. *Annu Rev Biochem* 1993; 62:797-  
3 821.
- 4 44. Voulgaridou GP, Anestopoulos I, Franco R, Panayiotidis MI, Pappa A. DNA  
5 damage induced by endogenous aldehydes: current state of knowledge. *Mutat Res*  
6 2011; 711:13-27.
- 7 45. Romero-Calvo I, Ocon B, Martinez-Moya P, Suarez MD, Zarzuelo A, Martinez-  
8 Augustin O, et al. Reversible Ponceau staining as a loading control alternative to  
9 actin in Western blots. *Anal Biochem* 2010; 401:318-20.
- 10 46. Rappold I, Iwabuchi K, Date T, Chen J. Tumor suppressor p53 binding protein 1  
11 (53BP1) is involved in DNA damage-signaling pathways. *J Cell Biol* 2001;  
12 153:613-20.
- 13 47. Wilson PF, Nham PB, Urbin SS, Hinz JM, Jones IM, Thompson LH. Inter-  
14 individual variation in DNA double-strand break repair in human fibroblasts  
15 before and after exposure to low doses of ionizing radiation. *Mutat Res* 2010;  
16 683:91-7.
- 17 48. Ugenskiene R, Prise K, Folkard M, Lekki J, Stachura Z, Zazula M, et al. Dose  
18 response and kinetics of foci disappearance following exposure to high- and low-  
19 LET ionizing radiation. *Int J Radiat Biol* 2009; 85:872-82.
- 20 49. Canman CE, Lim DS, Cimprich KA, Taya Y, Tamai K, Sakaguchi K, et al.  
21 Activation of the ATM kinase by ionizing radiation and phosphorylation of p53.  
22 *Science* 1998; 281:1677-9.

- 1 50. Valerie K, Yacoub A, Hagan MP, Curiel DT, Fisher PB, Grant S, et al. Radiation-  
2 induced cell signaling: inside-out and outside-in. *Molecular Can Ther* 2007;  
3 6:789-801.
- 4 51. Bohlen TT, Dosanjh M, Ferrari A, Gudowska I, Mairani A. FLUKA simulations  
5 of the response of tissue-equivalent proportional counters to ion beams for  
6 applications in hadron therapy and space. *Phys Med Biol* 2011; 56:6545-61.
- 7 52. Bohlen TT, Cerutti F, Dosanjh M, Ferrari A, Gudowska I, Mairani A, et al.  
8 Benchmarking nuclear models of FLUKA and GEANT4 for carbon ion therapy.  
9 *Phys Med Biol* 2010; 55:5833-47.
- 10 53. Managing Space Radiation Risk in the New Era of Space Exploration.  
11 Washington, D.C.: The National Academies Press; 2008.
- 12 54. Cucinotta F, Durante M. Cancer risk from exposure to galactic cosmic rays:  
13 implications for space exploration by human beings. *Lancet Oncol* 2006; 7:431-5.
- 14 55. Azzam EI, de Toledo SM, Little JB. Oxidative metabolism, gap junctions and the  
15 ionizing radiation-induced bystander effect. *Oncogene* 2003; 22:7050-7.
- 16 56. Anderson RG, Jacobson K. A role for lipid shells in targeting proteins to  
17 caveolae, rafts, and other lipid domains. *Science* 2002; 296:1821-5.
- 18 57. Poli G, Schaur RJ, Siems WG, Leonarduzzi G. 4-hydroxynonenal: a membrane  
19 lipid oxidation product of medicinal interest. *Med Res Rev* 2008; 28:569-631.
- 20 58. Petkau A. Role of superoxide dismutase in modification of radiation injury. *Br J*  
21 *Cancer Suppl* 1987; 8:87-95.

- 1 59. Spitz DR, Azzam EI, Li JJ, Gius D. Metabolic oxidation/reduction reactions and  
2 cellular responses to ionizing radiation: a unifying concept in stress response  
3 biology. *Cancer Metastasis Rev* 2004; 23:311-22.
- 4 60. Iliakis G. The role of DNA double strand breaks in ionizing radiation-induced  
5 killing of eukaryotic cells. *Bioessays* 1991; 13:641-8.
- 6 61. Asaithamby A, Uematsu N, Chatterjee A, Story MD, Burma S, Chen DJ. Repair  
7 of HZE-particle-induced DNA double-strand breaks in normal human fibroblasts.  
8 *Radiat Res* 2008; 169:437-46.
- 9 62. Northum JD, Guetersloh SB, Braby LA. FLUKA capabilities for microdosimetric  
10 analysis. *Radiat Res* 2012; 177:117-23.
- 11 63. Hamm RN, Wright HA, Katz R, Turner JE, Ritchie RH. Calculated yields and  
12 slowing-down spectra for electrons in liquid water: implications for electron and  
13 photon RBE. *Phys Med Biol* 1978; 23:1149-61.
- 14 64. Howell RW. Radiation spectra for Auger-electron emitting radionuclides: Report  
15 No. 2 of AAPM Nuclear Medicine Task Group No. 6. *Med Phys* 1992; 19:1371-  
16 83.
- 17 65. Jain MR, Li M, Chen W, Liu T, De Toledo SM, Pandey BN, et al. In vivo space  
18 radiation-induced non-targeted responses: late effects on molecular signaling in  
19 mitochondria. *Curr Mol Pharmacol* 2011; 4:106-14.
- 20 66. Blakely EA. New measurements for hadrontherapy and space radiation: biology.  
21 *Phys Med* 2001; 17 Suppl 1:50-8.



- 1 67. Little JB, Nagasawa H, Li GC, Chen DJ. Involvement of the nonhomologous end  
2 joining DNA repair pathway in the bystander effect for chromosomal aberrations.  
3 Radiat Res 2003; 159:262-7.
- 4 68. Mothersill C, Seymour RJ, Seymour CB. Bystander effects in repair-deficient cell  
5 lines. Radiat Res 2004; 161:256-63.
- 6 69. Azzam EI, de Toledo SM, Spitz DR, Little JB. Oxidative metabolism modulates  
7 signal transduction and micronucleus formation in bystander cells from alpha-  
8 particle-irradiated normal human fibroblast cultures. Cancer Res 2002; 62:5436-  
9 42.
- 10 70. Lorimore SA, Chrystal JA, Robinson JI, Coates PJ, Wright EG. Chromosomal  
11 instability in unirradiated hemaopoietic cells induced by macrophages exposed in  
12 vivo to ionizing radiation. Cancer Res 2008; 68:8122-6.
- 13 71. Cucinotta FA, Plante I, Ponomarev AL, Kim MH. Nuclear interactions in heavy  
14 ion transport and event-based risk models. Radiat Prot Dosimetry 2011; 143:384-  
15 90.
- 16 72. Meesungnoen J, Jay-Gerin J-P, Radiation chemistry of liquid water with heavy  
17 ions: Monte Carlo simulation studies. In *Charged Particle and Photon*  
18 *Interactions with Matter Recent Advances, Applications, and Interfaces* (Hatano  
19 Y, Katsumura Y, Mozumder A, Eds.), pp. 355-400. Taylor and Francis, Boca  
20 Raton, FL, 2011.
- 21 73. Turner JE, Magee JL, Wright HA, Chatterjee A, Hamm RN, Ritchie RH. Physical  
22 and chemical development of electron tracks in liquid water. Radiat Res 1983;  
23 96:437-49.
- 24

## FIGURE LEGENDS

**Figure 1.** Western blot analyses of p-TP53ser15, p-ERK1/2, p21<sup>Waf1</sup> and HDM2 in AG1522 cell populations at [A] 15 min, [B] 1 h, [C] 3 h, [D] 6 and 24 h after exposure to an absorbed dose of 0, 0.2 or 1 cGy from 1000 MeV/u <sup>56</sup>Fe ions, 600 MeV/u <sup>28</sup>Si ions or 3.7 MeV  $\alpha$  particles. Staining with Ponceau S Red was used as loading control. Each immunoblot is representative of 2-7 experiments. Fold change represents relative change compared to the control (i.e. 0 cGy).

**Figure 2.** Oxidative stress in confluent AG1522 cells harvested 24 h after exposure to low mean absorbed doses of 1000 MeV/u <sup>56</sup>Fe ion. Immunoblot analyses of [A] protein carbonylation, and [B] lipid peroxidation (measured by 4-HNE protein adduct accumulation). In the case of protein carbonylation, the relative intensity (i.e. fold-change) in oxidation of the overall spectrum of proteins (~30-130 kDa) in irradiated cells was compared to that in control cells. For 4-HNE protein adduct accumulation, the relative intensity refers to the level of the band with arrow relative to control. Staining with Ponceau S Red was used as loading control. Each immunoblot is representative of 3 experiments.

**Figure 3.** Western blot analyses of p21<sup>Waf1</sup>, p-TP53ser15 and HDM2 in AG1522 cell populations exposed to 1000 MeV/u <sup>56</sup>Fe ions. Confluent cells were exposed to a mean absorbed dose of 1 cGy and subcultured in fresh medium (1:3). Samples were harvested for analyses 8 and 24 h after irradiation. Staining with Ponceau S Red was used as loading control. Each immunoblot is representative of 3-5 experiments. Fold change represents relative change compared to the control.

**Figure 4.** Kinetics of 53BP1 foci formation in confluent AG1522 cell cultures exposed to 0.2 cGy from 1000 MeV/u  $^{56}\text{Fe}$  ions (Panel A), 3.7 MeV  $\alpha$  particles (Panel B) or 600 MeV/u  $^{28}\text{Si}$  ions (Panel C). The data represent the excess percent increase ( $\Delta F$ ) of cells with 53BP1 foci in irradiated cell populations relative to the respective control calculated as  $\Delta F = 100 (F_{\text{irradiated}} - F_{\text{control}})$  where F is the ratio of the number of cells with 53BP1 foci over the total number of cells counted. Each graph is representative of 3 different experiments.  $\chi^2$  test was performed on the total number of cells compared with respective control in irradiated populations. (\*:  $p < 0.05$  ; \*\*:  $p < 0.01$  ; \*\*\*:  $p < 0.001$ ).

**Figure 5.** Representative images of etched tracks and 53BP1 foci in AG1522 cell cultures grown on dishes with CR-39-nuclear track detector bottom. The cultures were fixed for analyses at 15 min after exposure to 0.2 cGy of 1000 MeV/u  $^{56}\text{Fe}$  ions: (A) visualization of etched tracks; (B) 53BP1 immuno-detection (red); (C) stained with DAPI; (D) images in A-C are super-imposed with the black dots representing etched tracks in (A) converted to white for better visualization.

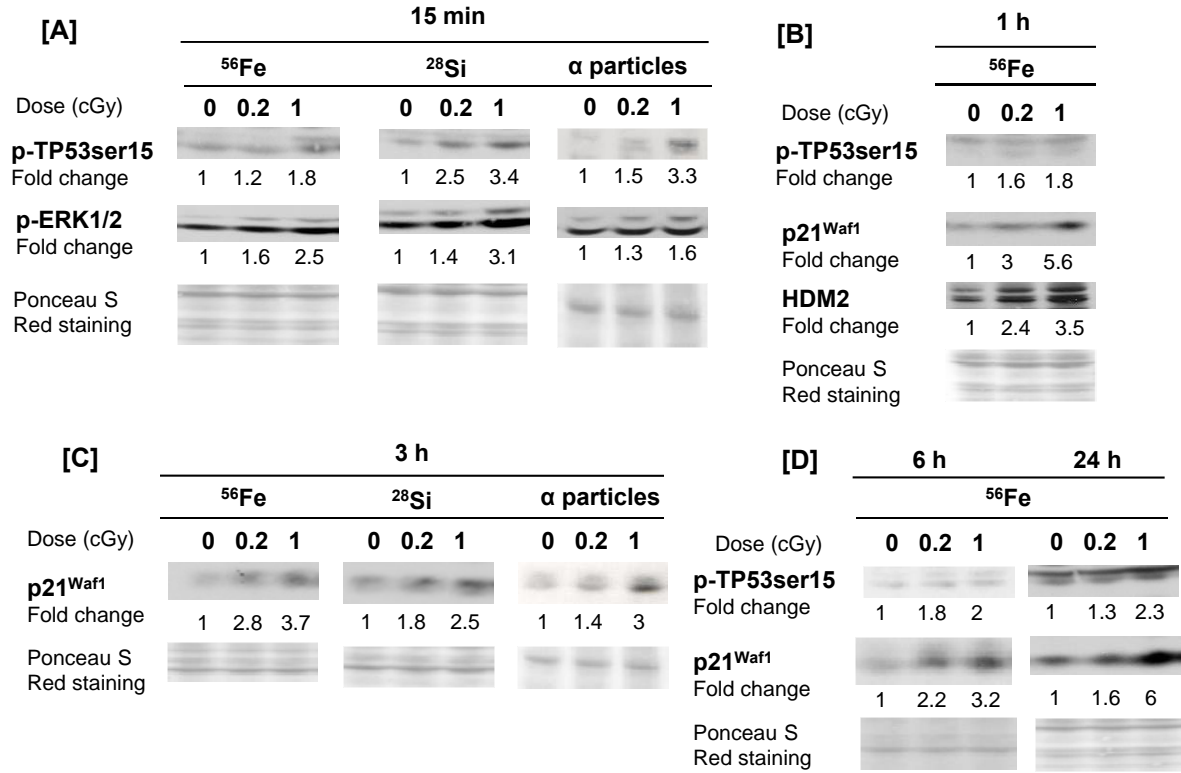
**Figure 6.** FLUKA simulation of radial distribution of dose, per primary irradiating particle, in 1  $\mu\text{m}$ -thick cell culture layer exposed to 0.2 cGy of 1000 MeV/u  $^{56}\text{Fe}$  ions. [A] Radial distribution of dose of  $^{56}\text{Fe}$  ions, heavy ions, 1 keV-threshold electrons and the total dose. [B] Radial distribution of dose of electrons with various  $\delta$  ray-thresholds (1, 10 and 100 keV and 1 MeV). Panels [C] and [D] illustrate radial distribution of dose from heavy ions (primary and secondary) and electrons, respectively, by superimposing the radial dose area over Panel D in Figure 5, where cells traversed by a primary  $^{56}\text{Fe}$  ion-track were identified.

1 **Supplementary Figure 1.** Schematics of tissue culture systems used in experiments. [A]  
2 Glass-bottomed flaskette (Nalge Nunc International). [B] Tissue culture dish with  
3 polyallyl diglycol carbonate (PADC, commonly known as Columbia Resin #39) plastic  
4 polymer bottom for HZE-particle-irradiation. Incorporation of a 100  $\mu\text{m}$ -thick PADC  
5 film below the glass bottom of the sealable-dish permits visualization of HZE-particle-  
6 tracks without interfering with microscopic examination of biological changes. The  
7 dishes filled to capacity with pH- and temperature-equilibrated growth medium can be  
8 positioned perpendicularly to the incident beam.  
9

## FOOTNOTES

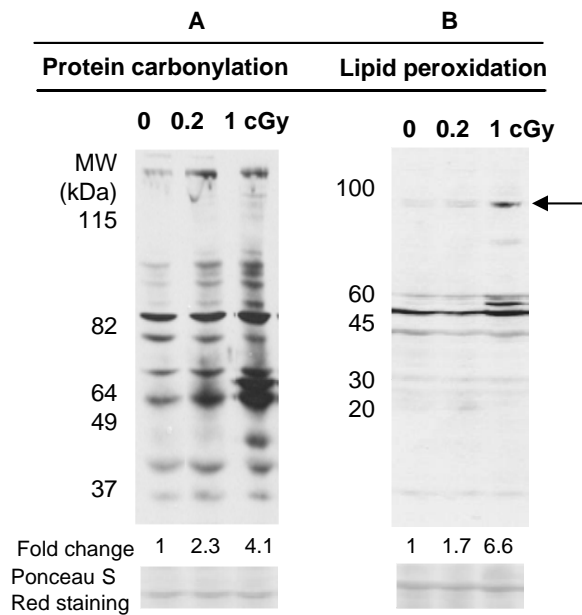
- <sup>1</sup> The thickness of  $\sim 1 \mu\text{m}$  of an AG1522 cell (41) was estimated from studies in fixed/dehydrated cells grown on Mylar. The actual dimension of a live AG1522 cell grown on glass may be different.
- <sup>2</sup> The absorbed dose ( $d$ ) per traversal to the thin disk-shaped cell nucleus of the AG1522 cell was calculated according to the relation  $d = (0.16 \text{ LET})/(A \rho)$ , where  $A$  is the cross-sectional area of the cell nucleus (i.e. an average of  $\sim 140 \mu\text{m}^2$ ), and  $\rho$  is the density of the cell.

*In confluent cell cultures*



*In confluent cell cultures*

**Oxidative Stress Dose Response to <sup>56</sup>Fe ions**

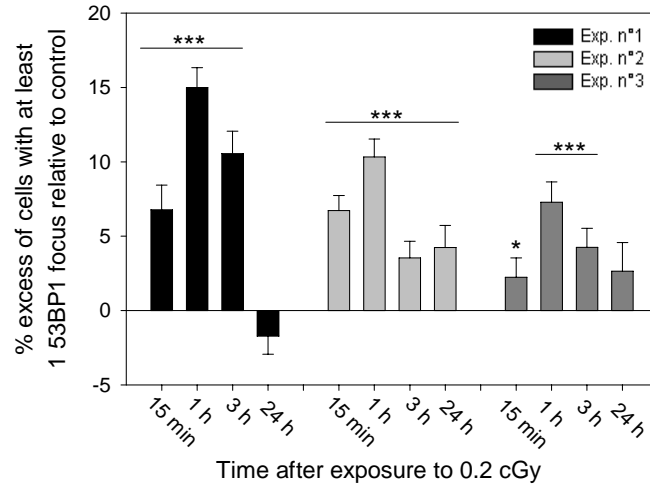


*In proliferating cells*

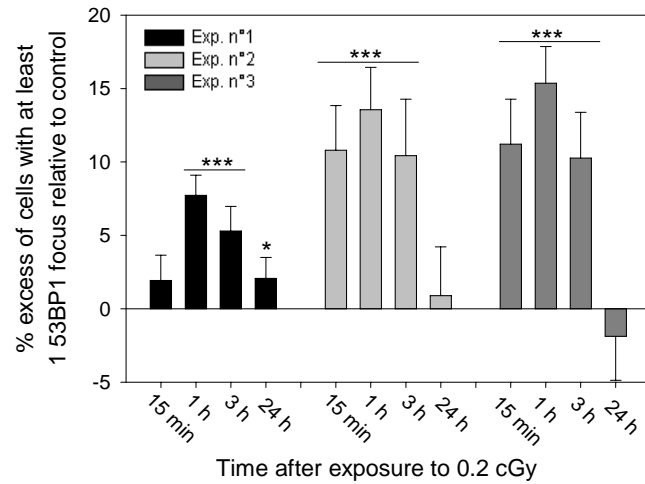
	8 h		24 h	
	<sup>56</sup> Fe			
Dose (cGy)	0	1	0	1
<b>p-TP53ser15</b>				
Fold change	1	1.4	1	1.5
<b>p21<sup>Waf1</sup></b>				
Fold change	1	2.4	1	1.8
<b>HDM2</b>				
<i>Fold change</i>	1	1.8	1	1.5
Ponceau S				
Red staining				



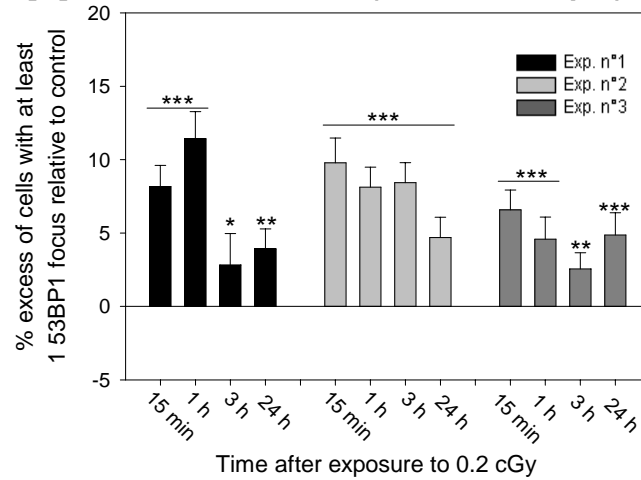
**[A] 1000 MeV/u  $^{56}\text{Fe}$  ions (LET ~151 keV/ $\mu\text{m}$ )**

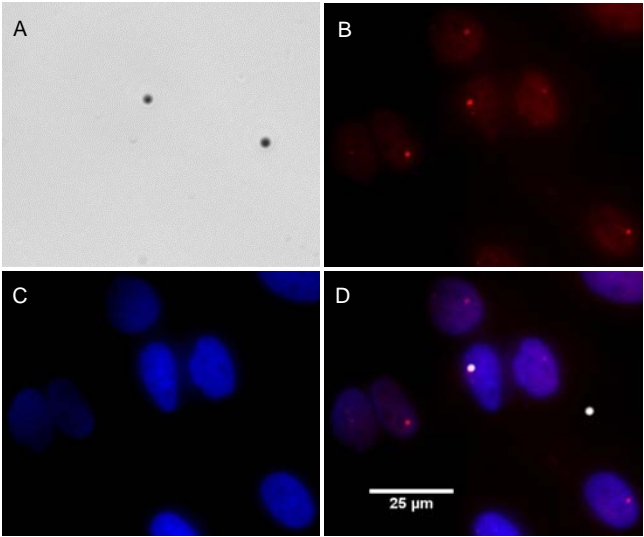


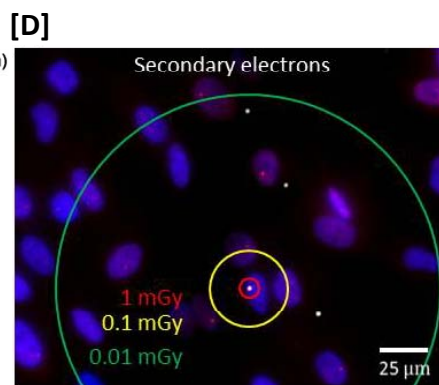
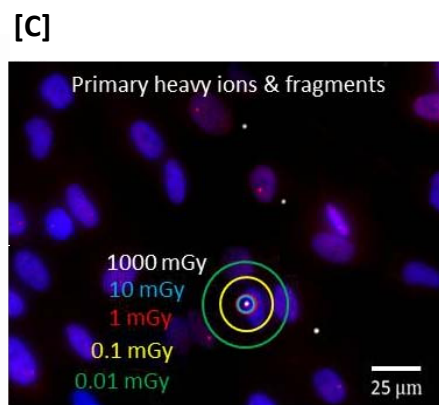
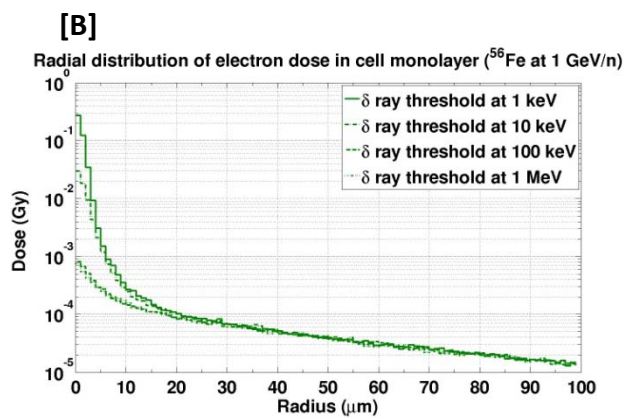
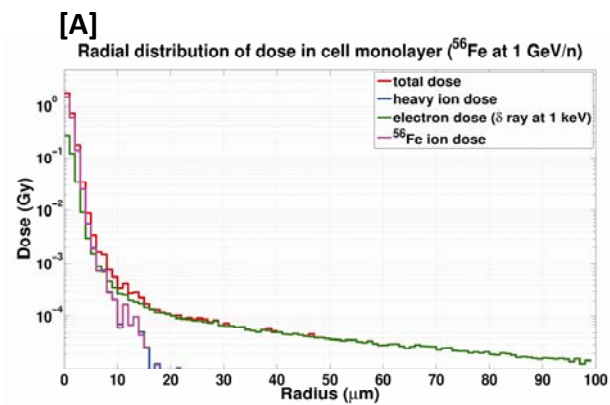
**[B] 3.7 MeV  $\alpha$  particles (LET ~109 keV/ $\mu\text{m}$ )**



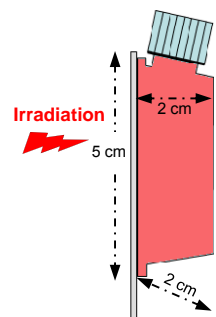
**[C] 600 MeV/u  $^{28}\text{Si}$  ions (LET ~50 keV/ $\mu\text{m}$ )**







[A] Glass-bottomed flaskette



[B] Tissue culture dish with 100  $\mu\text{m}$ -thick PADC plastic grafted

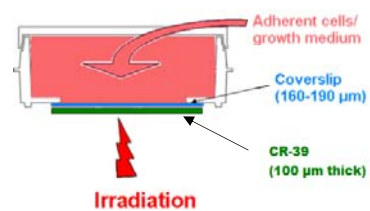


**Table 1: Estimates<sup>a</sup> of particle traversals when confluent AG1522 normal human fibroblasts are exposed to mean absorbed dose of 0.2 cGy from radiations that differ in their energy and linear energy transfer (LET)**

Ion <sup>b</sup>	Energy (MeV/u)	LET (keV/μm)	Dose (cGy)	Fluence (particles/cm <sup>2</sup> )	Average number of traversals		Fraction of cell nuclei traversed by 0, 1 or more than 1 particles		
					Cell	Nucleus	P(0)	P(1)	P(≥2)
<sup>56</sup> Fe <sup>26+</sup>	1000	151	0.2	$8.27 \times 10^3$	0.066	0.012	0.988	0.011	0.001
			1.0	$4.13 \times 10^4$	0.331	0.058	0.944	0.055	0.001
<sup>28</sup> Si <sup>14+</sup>	600	50	0.2	$2.50 \times 10^4$	0.200	0.035	0.966	0.033	0.001
			1.0	$1.25 \times 10^5$	0.999	0.175	0.840	0.147	0.013
<sup>12</sup> C <sup>6+</sup>	290	13	0.2	$9.60 \times 10^4$	0.768	0.134	0.874	0.118	0.008
			1.0	$4.80 \times 10^5$	3.841	0.672	0.511	0.343	0.146
<sup>4</sup> He <sup>2+</sup> (α)	0.92	109	0.2	$1.15 \times 10^4$	0.092	0.016	0.984	0.016	0.000
			1.0	$5.72 \times 10^4$	0.458	0.080	0.923	0.074	0.003

<sup>a</sup> These estimates do not take into account secondary radiations.

<sup>b</sup> Note that the primary ions are stripped of electrons. The charge is implied, but not designated, elsewhere in this publication.

**Table 2: Contribution of primary and secondary particles to the mean absorbed dose in the *cell monolayer* (0.001 cm<sup>3</sup>) when 1000 MeV/u <sup>56</sup>Fe, 600 MeV/u <sup>28</sup>Si, or 290 MeV/u <sup>12</sup>C ions are used to deliver 0.2 cGy to the AG1522 cell culture.**

	<sup>56</sup> Fe		<sup>28</sup> Si		<sup>12</sup> C	
<b>Particles<sup>a</sup></b>	Absorbed Dose <sup>b</sup> (cGy)	Contribution to total dose (%)	Absorbed Dose <sup>b</sup> (cGy)	Contribution to total dose (%)	Absorbed Dose <sup>b</sup> (cGy)	Contribution to total dose (%)
HZE primary	0.1221	59.87	0.1232	60.96	0.1268	62.06
HZE fragments	0.0007	0.35	0.0004	0.20	0.0002	0.09
Electrons	0.0807	39.57	0.0777	38.44	0.0755	36.94
Photons	2.2013 x 10 <sup>-6</sup>	0.00	1.1169 x 10 <sup>-6</sup>	0.00	8.7095 x 10 <sup>-7</sup>	0.00
Protons	2.3514 x 10 <sup>-4</sup>	0.12	4.7413 x 10 <sup>-4</sup>	0.23	1.0729 x 10 <sup>-3</sup>	0.53
Alpha	5.1070 x 10 <sup>-5</sup>	0.03	1.4144 x 10 <sup>-4</sup>	0.07	3.5004 x 10 <sup>-4</sup>	0.17
<b>Total</b>	<b>0.2039</b>	<b>100.00</b>	<b>0.2021</b>	<b>100.00</b>	<b>0.2043</b>	<b>100</b>

<sup>a</sup> Production thresholds for  $\delta$  rays were set at 1 keV. Transport cut-offs were set at 150 eV for electrons and 1 keV for HZE particles, protons, photons and  $\alpha$  particles.

<sup>b</sup> Errors in the absorbed doses are detailed in Supplementary Tables 2-4.

**Supplementary Table 1: Results of Western Blot analyses of p-TP53ser15, p-ERK1/2, p21<sup>Waf1</sup>, HDM2, protein carbonylation and lipid peroxidation related to the data in [A] Figure 1, [B] Figure 2 and [C] Figure 3, after exposure of AG1522 cells to an absorbed dose of 0, 0.2 or 1 cGy from 1000 MeV/u <sup>56</sup>Fe ions, 600 MeV/u <sup>28</sup>Si ions or 3.7 MeV  $\alpha$  particles.**

**The number of individual experiment, averaged data and associated errors are noted.**

**[A] In confluent cell cultures**

<i>Particles</i>	<i>Dose</i>	<i>Time</i>	<i>Protein</i>	<i>Fold increase relative to control</i>	<i>n</i>	<i>Mean</i>	<i>Standard Error (SE)</i>
3.7 MeV $\alpha$ particles	0.2 cGy	15 min	p-TP53ser15	1.5/1.4/1.4/1.5	4	1.5	0.0
	0.2 cGy	15 min	p-ERK1/2	1.3/1.2/1.1	3	1.2	0.1
	0.2 cGy	3 h	p21 <sup>Waf1</sup>	1.4/2/1.6	3	1.7	0.2
	1 cGy	15 min	p-TP53ser15	3.3/1.8/2/1.5/2.8/1.7/1.6	7	2.1	0.3
	1 cGy	15 min	p-ERK1/2	1.6/2/2.2/1.8/2.9/2.4	6	2.2	0.2
	1 cGy	3 h	p21 <sup>Waf1</sup>	3/1.6/3.6/2.6/2.4/3	6	2.7	0.3
1000 MeV/u <sup>56</sup> Fe ions	0.2 cGy	15 min	p-TP53ser15	1.2/1.3/2.5	3	1.7	0.4
	0.2 cGy	15 min	p-ERK1/2	1.6/1.2/1.3	3	1.4	0.1
	0.2 cGy	1 h	HDM2	2.4/1.5/2.2	3	2.0	0.3
	0.2 cGy	1 h	p21 <sup>Waf1</sup>	3/3.2/1.5	3	2.6	0.5
	0.2 cGy	1 h	p-TP53ser15	1.6/1.5/1.4	3	1.5	0.1
	0.2 cGy	3 h	p21 <sup>Waf1</sup>	2.8/1.7/1.2/1.6/1.3	5	1.7	0.3
	0.2 cGy	6 h	p-TP53ser15	1.8/1.2	2	1.5	0.3
	0.2 cGy	6 h	p21 <sup>Waf1</sup>	2.2/1.2/1.7	3	1.7	0.3
	0.2 cGy	24 h	p21 <sup>Waf1</sup>	1.6/1.2/1.4	3	1.4	0.1
	0.2 cGy	24 h	p-TP53ser15	1.3/1.4/1.4	3	1.4	0.0
	1 cGy	15 min	p-TP53ser15	1.8/2.4/1.8/7.9/2.8/2.6	6	3.2	1.0
	1 cGy	15 min	p-ERK1/2	2.5/2.9/2.2/4/2.1	5	2.7	0.3
	1 cGy	1 h	HDM2	3.5/2.3/2.2/2.5/2.5/1.4	6	2.4	0.3
	1 cGy	1 h	p21 <sup>Waf1</sup>	5.6/1.8/1.6	3	3.0	1.3
	1 cGy	1 h	p-TP53ser15	1.8/1.6/2.6	3	2	0.3
	1 cGy	3 h	p21 <sup>Waf1</sup>	3.7/2/2.5/1.7/2.4	5	2.5	0.3
	1 cGy	6 h	p-TP53ser15	2/2.3	2	2.2	0.2
	1 cGy	6 h	p21 <sup>Waf1</sup>	3.2/2.4/1.3	3	2.3	0.6
	1 cGy	24 h	p21 <sup>Waf1</sup>	6/3.7/5	3	4.9	0.7
	1 cGy	24 h	p-TP53ser15	2.3/5.1/2.2	3	3.2	1.0
600 MeV/u <sup>28</sup> Si ions	0.2 cGy	15 min	p-TP53ser15	2.5/3.1/1.3	3	2.3	0.5
	0.2 cGy	15 min	p-ERK1/2	1.4/1.5/1.2	3	1.4	0.1
	0.2 cGy	3 h	p21 <sup>Waf1</sup>	1.8/1.2/1.1	3	1.4	0.2
	1 cGy	15 min	p-TP53ser15	3.4/2.4/1.6/4	4	2.9	0.5
	1 cGy	15 min	p-ERK1/2	3.1/2.1/2.8/1.6	4	2.4	0.3
	1 cGy	3 h	p21 <sup>Waf1</sup>	2.5/2.3/2.2	3	2.3	0.1

**[B] In confluent cell cultures**

<i>Particles</i>	<i>Dose</i>	<i>Time</i>	<i>Protein</i>	<i>Fold increase relative to control</i>	<i>n</i>	<i>Mean</i>	<i>Standard Error (SE)</i>
1000 MeV/u <sup>56</sup> Fe ions	0.2 cGy	24 h	Protein Carbonylation	2.3/6/1.5	3	3.3	1.4
	0.2 cGy	24 h	Lipid peroxydation	1.7/1.4/2.2	3	1.8	0.2
	1 cGy	24 h	Protein Carbonylation	4.1/10/5.5	3	6.5	1.8
	1 cGy	24 h	Lipid peroxydation	6.6/2.1/2.8	3	3.8	1.4

**[C] In proliferating cells**

<i>Particles</i>	<i>Dose</i>	<i>Time</i>	<i>Protein</i>	<i>Fold increase relative to control</i>	<i>n</i>	<i>Mean</i>	<i>Standard Error (SE)</i>
1000 MeV/u <sup>56</sup> Fe ions	1 cGy	8 h	p-TP53ser15	1.4/1.2/1.5/1.9	4	1.5	0.1
	1 cGy	8 h	p21 <sup>Waf1</sup>	2.4/1.3/1.4/1.8/1.8	5	1.7	0.2
	1 cGy	8 h	HDM2	1.8/1.7/1.6	3	1.7	0.1
	1 cGy	24 h	p-TP53ser15	1.5/1.2/2.3/1.3	4	1.6	0.2
	1 cGy	24 h	p21 <sup>Waf1</sup>	1.8/2.1/1.5/1.1	4	1.6	0.2
	1 cGy	24 h	HDM2	1.5/2.5/1.1/2.7/1.3	5	1.8	0.3



**Supplementary Table 2: Contribution of primary and secondary particles to the mean absorbed dose in the glass coverslip, cell culture and medium when 1000 MeV/u  $^{56}\text{Fe}$  ions were used to deliver 0.2 cGy to the AG1522 cell culture. The production thresholds of  $\delta$  rays were set at [A] 1 keV, [B] 10 keV, [C] 100 keV, [D] 1 MeV. The transport cut-off was set at 1 keV for HZE particles, protons, photons, and  $\alpha$  particles. For electrons, it was set at 150 eV (Panel A) or 1 keV (Panels B, C and D).**

**[A]**

<b>1 keV</b>	<b>Glass coverslip (1.9152 cm<sup>3</sup>)</b>	<b>Cell Monolayer (0.001 cm<sup>3</sup>)</b>		<b>Medium (water) (18.799 cm<sup>3</sup>)</b>
<b>Particles</b>	<b>Absorbed Dose (cGy)</b>	<b>Absorbed Dose (cGy)</b>	<b>Contribution to total dose %</b>	<b>Absorbed Dose (cGy)</b>
Total heavy ions	0.1000 $\pm$ 0.0007	0.1228 $\pm$ 0.0022	60.22 0.35	0.1185 $\pm$ 0.0022
$^{56}\text{Fe}$ ions	0.0997 $\pm$ 0.0007	0.1221 $\pm$ 0.0022	59.87	0.1114 $\pm$ 0.0022
Electrons	0.0623 $\pm$ 0.0004	0.0807 $\pm$ 0.0014	39.57	0.0756 $\pm$ 0.0014
Photons	3.2609 $\times 10^{-6} \pm 0.69$ %	2.2013 $\times 10^{-6} \pm 82.22$ %	0.00	2.3844 $\times 10^{-6} \pm 1.11$ %
Protons	1.2438 $\times 10^{-4} \pm 8.72$ %	2.3514 $\times 10^{-4} \pm 21.97$ %	0.12	5.1421 $\times 10^{-4} \pm 2.57$ %
Alpha	4.3250 $\times 10^{-5} \pm 16.40$ %	5.1070 $\times 10^{-5} \pm 102.92$ %	0.03	1.5104 $\times 10^{-4} \pm 3.47$ %
<b>Total</b>	<b>0.1626 <math>\pm</math> 0.0012</b>	<b>0.2039 <math>\pm</math> 0.0036</b>	<b>100</b>	<b>0.1950 <math>\pm</math> 0.0036</b>

**[B]**

<b>10 keV</b>	<b>Glass coverslip (1.9152 cm<sup>3</sup>)</b>	<b>Cell Monolayer (0.001 cm<sup>3</sup>)</b>		<b>Medium (water) (18.799 cm<sup>3</sup>)</b>
<b>Particles</b>	<b>Absorbed Dose (cGy)</b>	<b>Absorbed Dose (cGy)</b>	<b>Contribution to total dose %</b>	<b>Absorbed Dose (cGy)</b>
Total heavy ions	0.1206 $\pm$ 0.0011	0.1452 $\pm$ 0.0020	71.67 0.44	0.1404 $\pm$ 0.0019
$^{56}\text{Fe}$ ions	0.1202 $\pm$ 0.0011	0.1443 $\pm$ 0.0020	71.23	0.1320 $\pm$ 0.0018
Electrons	0.0412 $\pm$ 0.0004	0.0569 $\pm$ 0.0009	28.08	0.0529 $\pm$ 0.0007
Photons	2.7719 $\times 10^{-6} \pm 0.92$ %	1.9991 $\times 10^{-6} \pm 14.62$ %	0.00	2.1064 $\times 10^{-6} \pm 1.35$ %
Protons	1.6855 $\times 10^{-4} \pm 7.96$ %	2.8335 $\times 10^{-4} \pm 16.52$ %	0.14	6.1175 $\times 10^{-4} \pm 3.49$ %
Alpha	5.7126 $\times 10^{-5} \pm 16.36$ %	9.6370 $\times 10^{-5} \pm 57.56$ %	0.05	1.7112 $\times 10^{-4} \pm 4.38$ %
<b>Total</b>	<b>0.1622 <math>\pm</math> 0.0015</b>	<b>0.2025 <math>\pm</math> 0.0029</b>	<b>100</b>	<b>0.1943 <math>\pm</math> 0.0026</b>

[C]

100 keV	Glass coverslip (1.9152 cm <sup>3</sup> )	Cell Monolayer (0.001 cm <sup>3</sup> )		Medium (water) (18.799 cm <sup>3</sup> )
Particles	Absorbed Dose (cGy)	Absorbed Dose (cGy)	Contribution to total dose %	Absorbed Dose (cGy)
Total heavy ions	0.1420 ± 0.0008	0.1698 ± 0.0018	84.94 0.48	0.1642 ± 0.0018
<sup>56</sup> Fe ions	0.1416 ± 0.0008	0.1688 ± 0.0018	84.46	0.1546 ± 0.0016
Electrons	0.0198 ± 0.0001	0.0294 ± 0.0004	14.72	0.0301 ± 0.0003
Photons	1.5099 x 10 <sup>-6</sup> ± 0.79 %	1.0620 x 10 <sup>-6</sup> ± 74.71 %	0.00	1.3329 x 10 <sup>-6</sup> ± 2.33 %
Protons	1.8447 x 10 <sup>-4</sup> ± 8.36 %	3.5205 x 10 <sup>-4</sup> ± 12.33 %	0.18	7.0077 x 10 <sup>-4</sup> ± 2.84 %
Alpha	5.6496 x 10 <sup>-5</sup> ± 13.10 %	1.5287 x 10 <sup>-4</sup> ± 98.28 %	0.08	1.9140 x 10 <sup>-4</sup> ± 4.40 %
<b>Total</b>	<b>0.1622 ± 0.0009</b>	<b>0.1999 ± 0.0021</b>	<b>100</b>	<b>0.1954 ± 0.0021</b>

[D]

1 MeV	Glass coverslip (1.9152 cm <sup>3</sup> )	Cell Monolayer (0.001 cm <sup>3</sup> )		Medium (water) (18.799 cm <sup>3</sup> )
Particles	Absorbed Dose (cGy)	Absorbed Dose (cGy)	Contribution to total dose %	Absorbed Dose (cGy)
Total heavy ions	0.1633 ± 0.0008	0.1922 ± 0.0027	97.66 0.61	0.1858 ± 0.0016
<sup>56</sup> Fe ions	0.1628 ± 0.0008	0.1910 ± 0.0028	97.05	0.1751 ± 0.0016
Electrons	0.0016 ± 0.72 %	0.0040 ± 0.0001	2.03	0.0069 ± 0.0001
Photons	3.0758 x 10 <sup>-7</sup> ± 2.36 %	4.9817 x 10 <sup>-8</sup> ± 75.16 %	0.00003	1.7904 x 10 <sup>-7</sup> ± 14.80 %
Protons	2.0372 x 10 <sup>-4</sup> ± 7.36 %	3.4352 x 10 <sup>-4</sup> ± 8.05 %	0.17	7.4120 x 10 <sup>-4</sup> ± 3.54 %
Alpha	6.1595 x 10 <sup>-5</sup> ± 12.03 %	1.1259 x 10 <sup>-4</sup> ± 78.06 %	0.05	2.0916 x 10 <sup>-4</sup> ± 4.68 %
<b>Total</b>	<b>0.1653 ± 0.0008</b>	<b>0.1968 ± 0.0029</b>	<b>100</b>	<b>0.1939 ± 0.0016</b>

Errors represent standard deviations of the mean. When the standard deviation is < 0.0001 cGy, it is expressed and noted in % as it can represent a high deviation. The term “total heavy ion” refers to the primary 1000 MeV/u <sup>56</sup>Fe ions and the fragments.

**Supplementary Table 3: Contribution of primary and secondary particles to the mean absorbed dose in the glass coverslip, cell culture and medium when 600 MeV/u  $^{28}\text{Si}$  ions were used to deliver 0.2 cGy to the AG1522 cell culture. The production thresholds of  $\delta$  rays were set at [A] 1 keV, [B] 10 keV, [C] 100 keV, [D] 1 MeV. The transport cut-off was set at 1 keV for HZE particles, protons, photons, and  $\alpha$  particles. For electrons, it was set at 150 eV (Panel A) or 1 keV (Panels B, C and D).**

**[A]**

<b>1 keV</b>	<b>Glass coverslip (1.9152 cm<sup>3</sup>)</b>	<b>Cell Monolayer (0.001 cm<sup>3</sup>)</b>		<b>Medium (water) (18.799 cm<sup>3</sup>)</b>
<b>Particles</b>	<b>Absorbed Dose (cGy)</b>	<b>Absorbed Dose (cGy)</b>	<b>Contribution to total dose %</b>	<b>Absorbed Dose (cGy)</b>
Total heavy ions	0.1006 $\pm$ 0.0003	0.1236 $\pm$ 0.0012	61.16 0.20	0.1209 $\pm$ 0.0004
$^{28}\text{Si}$ ions	0.1003 $\pm$ 0.0010	0.1232 $\pm$ 0.0012	60.96	0.1170 $\pm$ 0.0012
Electrons	0.0611 $\pm$ 0.0006	0.0777 $\pm$ 0.0012	38.44	0.0720 $\pm$ 0.0007
Photons	3.1033 $\times 10^{-6} \pm 1.40$ %	1.1169 $\times 10^{-6} \pm 82.11$ %	0.00	2.1527 $\times 10^{-6} \pm 2.25$ %
Protons	2.7759 $\times 10^{-4} \pm 5.06$ %	4.7413 $\times 10^{-4} \pm 26.76$ %	0.23	9.7519 $\times 10^{-4} \pm 5.20$ %
Alpha	1.0644 $\times 10^{-4} \pm 13.94$ %	1.4144 $\times 10^{-4} \pm 73.98$ %	0.07	2.6864 $\times 10^{-4} \pm 5.03$ %
<b>Total</b>	<b>0.1622 <math>\pm</math> 0.0016</b>	<b>0.2021 <math>\pm</math> 0.0024</b>	<b>100</b>	<b>0.1945 <math>\pm</math> 0.0019</b>

**[B]**

<b>10 keV</b>	<b>Glass coverslip (1.9152 cm<sup>3</sup>)</b>	<b>Cell Monolayer (0.001 cm<sup>3</sup>)</b>		<b>Medium (water) (18.799 cm<sup>3</sup>)</b>
<b>Particles</b>	<b>Absorbed Dose (cGy)</b>	<b>Absorbed Dose (cGy)</b>	<b>Contribution to total dose %</b>	<b>Absorbed Dose (cGy)</b>
Total heavy ions	0.1218 $\pm$ 0.0008	0.1467 $\pm$ 0.0014	73.11 0.26	0.1436 $\pm$ 0.0016
$^{28}\text{Si}$ ions	0.1215 $\pm$ 0.0008	0.1462 $\pm$ 0.0014	72.85	0.1389 $\pm$ 0.0016
Electrons	0.0392 $\pm$ 0.0003	0.0531 $\pm$ 0.0009	26.44	0.0479 $\pm$ 0.0005
Photons	2.5971 $\times 10^{-6} \pm 0.75$ %	1.0276 $\times 10^{-6} \pm 54.41$ %	0.00	1.8470 $\times 10^{-6} \pm 2.18$ %
Protons	3.4229 $\times 10^{-4} \pm 7.30$ %	5.7103 $\times 10^{-4} \pm 22.19$ %	0.28	1.2144 $\times 10^{-3} \pm 3.40$ %
Alpha	1.2456 $\times 10^{-4} \pm 8.93$ %	1.0788 $\times 10^{-4} \pm 82.28$ %	0.05	3.4464 $\times 10^{-4} \pm 4.14$ %
<b>Total</b>	<b>0.1617 <math>\pm</math> 0.0010</b>	<b>0.2007 <math>\pm</math> 0.0023</b>	<b>100</b>	<b>0.1934 <math>\pm</math> 0.0021</b>

[C]

100 keV	Glass coverslip (1.9152 cm <sup>3</sup> )	Cell Monolayer (0.001 cm <sup>3</sup> )		Medium (water) (18.799 cm <sup>3</sup> )
Particles	Absorbed Dose (cGy)	Absorbed Dose (cGy)	Contribution to total dose %	Absorbed Dose (cGy)
Total heavy ions	0.1434 ± 0.0004	0.1708 ± 0.0011	86.74 0.31	0.1671 ± 0.0014
<sup>28</sup> Si ions	0.1431 ± 0.0012	0.1702 ± 0.0011	86.43	0.1616 ± 0.0013
Electrons	0.0175 ± 0.0001	0.0250 ± 0.0003	12.70	0.0241 ± 0.0002
Photons	1.3178 x 10 <sup>-6</sup> ± 0.90 %	6.7873 x 10 <sup>-7</sup> ± 157.79 %	0.00	1.0610 x 10 <sup>-6</sup> ± 2.89 %
Protons	3.9845 x 10 <sup>-4</sup> ± 7.79 %	7.0894 x 10 <sup>-4</sup> ± 14.22 %	0.36	1.3842 x 10 <sup>-3</sup> ± 1.63 %
Alpha	1.3043 x 10 <sup>-4</sup> ± 12.69 %	1.8740 x 10 <sup>-4</sup> ± 67.54 %	0.10	3.4464 x 10 <sup>-4</sup> ± 4.14 %
<b>Total</b>	<b>0.1616 ± 0.0014</b>	<b>0.1969 ± 0.0013</b>	<b>100</b>	<b>0.1933 ± 0.0016</b>

[D]

1 MeV	Glass coverslip (1.9152 cm <sup>3</sup> )	Cell Monolayer (0.001 cm <sup>3</sup> )		Medium (water) (18.799 cm <sup>3</sup> )
Particles	Absorbed Dose (cGy)	Absorbed Dose (cGy)	Contribution to total dose %	Absorbed Dose (cGy)
Total heavy ions	0.1633 ± 0.0012	0.1938 ± 0.0041	98.43 0.36	0.1887 ± 0.0030
<sup>28</sup> Si ions	0.1630 ± 0.0122	0.1931 ± 0.0409	98.07	0.1827 ± 0.0296
Electrons	0.0007 ± 0.0000	0.0019 ± 0.0001	0.96	0.0027 ± 0.0000
Photons	1.4358 x 10 <sup>-7</sup> ± 5.34 %	1.8106 x 10 <sup>-8</sup> ± 210.82 %	0.00	6.5495 x 10 <sup>-8</sup> ± 20.30 %
Protons	3.7917 x 10 <sup>-4</sup> ± 9.00 %	6.5103 x 10 <sup>-4</sup> ± 14.40 %	0.48	1.4250 x 10 <sup>-3</sup> ± 3.29 %
Alpha	1.3149 x 10 <sup>-4</sup> ± 11.76 %	1.1953 x 10 <sup>-4</sup> ± 38.38 %	0.06	3.8005 x 10 <sup>-4</sup> ± 4.26 %
<b>Total</b>	<b>0.1647 ± 0.0012</b>	<b>0.1969 ± 0.0041</b>	<b>100</b>	<b>0.1937 ± 0.0031</b>

Errors represent standard deviations of the mean. When the standard deviation is <0.0001 cGy, it is expressed and noted in % as it can represent a high deviation. The term “total heavy ion” refers to the primary 600 MeV/u <sup>28</sup>Si ions and the fragments.

**Supplementary Table 4: Contribution of primary and secondary particles to the mean absorbed dose in the glass coverslip, cell culture and medium when 290 MeV/u  $^{12}\text{C}$  ions are used to deliver 0.2 cGy to the AG1522 cell culture. The production thresholds of  $\delta$  rays were set at [A] 1 keV, [B] 10 keV, [C] 100 keV, [D] 1 MeV. The transport cut-off was set at 1 keV for HZE particles, protons, photons and  $\alpha$  particles. For electrons, it was set at 150 eV (Panel A) or 1 keV (Panels B, C and D).**

**[A]**

<b>1 keV</b>	<b>Glass coverslip (1.9152 cm<sup>3</sup>)</b>	<b>Cell Monolayer (0.001 cm<sup>3</sup>)</b>		<b>Medium (water) (18.799 cm<sup>3</sup>)</b>
<b>Particles</b>	<b>Absorbed Dose (cGy)</b>	<b>Absorbed Dose (cGy)</b>	<b>Contribution to total dose %</b>	<b>Absorbed Dose (cGy)</b>
Total heavy ions	0.1024 ± 0.0001	0.1270 ± 0.0013	62.15 0.09	0.1265 ± 0.0001
$^{12}\text{C}$ ions	0.1023 ± 0.0006	0.1268 ± 0.0013	62.06	0.1249 ± 0.0011
Electrons	0.0613 ± 0.0004	0.0755 ± 0.0015	36.94	0.0710 ± 0.0006
Photons	3.0082 x 10 <sup>-6</sup> ± 0.93 %	8.7095 x 10 <sup>-7</sup> ± 138.13 %	0.00	1.9454 x 10 <sup>-6</sup> ± 2.67 %
Protons	6.0239 x 10 <sup>-4</sup> ± 10.79 %	1.0729 x 10 <sup>-3</sup> ± 34.90 %	0.53	2.2658 x 10 <sup>-3</sup> ± 4.59 %
Alpha	2.6778 x 10 <sup>-4</sup> ± 15.20 %	3.5004 x 10 <sup>-4</sup> ± 84.32 %	0.17	7.1590 x 10 <sup>-4</sup> ± 4.49 %
<b>Total</b>	<b>0.1649 ± 0.0011</b>	<b>0.2043 ± 0.0029</b>	<b>100</b>	<b>0.2011 ± 0.0018</b>

**[B]**

<b>10 keV</b>	<b>Glass coverslip (1.9152 cm<sup>3</sup>)</b>	<b>Cell Monolayer (0.001 cm<sup>3</sup>)</b>		<b>Medium (water) (18.799 cm<sup>3</sup>)</b>
<b>Particles</b>	<b>Absorbed Dose (cGy)</b>	<b>Absorbed Dose (cGy)</b>	<b>Contribution to total dose %</b>	<b>Absorbed Dose (cGy)</b>
Total heavy ions	0.1256 ± 0.0010	0.1525 ± 0.0019	74.89 0.21	0.1521 ± 0.0019
$^{12}\text{C}$ ions	0.1254 ± 0.0010	0.1521 ± 0.0020	74.68	0.1501 ± 0.0019
Electrons	0.0378 ± 0.0003	0.0490 ± 0.0009	24.05	0.0443 ± 0.0005
Photons	2.4343 x 10 <sup>-6</sup> ± 1.24 %	9.3402 x 10 <sup>-7</sup> ± 105.77 %	0.00	1.6359 x 10 <sup>-6</sup> ± 4.67 %
Protons	7.7265 x 10 <sup>-4</sup> ± 14.18 %	1.3566 x 10 <sup>-3</sup> ± 36.62 %	0.67	2.7321 x 10 <sup>-3</sup> ± 4.26 %
Alpha	3.5199 x 10 <sup>-4</sup> ± 13.32 %	2.3531 x 10 <sup>-4</sup> ± 98.87 %	0.12	7.0770 x 10 <sup>-4</sup> ± 5.66 %
<b>Total</b>	<b>0.1648 ± 0.0013</b>	<b>0.2037 ± 0.0030</b>	<b>100</b>	<b>0.2007 ± 0.0024</b>

[C]

100 keV	Glass coverslip (1.9152 cm <sup>3</sup> )	Cell Monolayer (0.001 cm <sup>3</sup> )		Medium (water) (18.799 cm <sup>3</sup> )
Particles	Absorbed Dose (cGy)	Absorbed Dose (cGy)	Contribution to total dose %	Absorbed Dose (cGy)
Total heavy ions	0.1489 ± 0.0001	0.1787 ± 0.0033	88.92 0.20	0.1772 ± 0.0015
<sup>12</sup> C ions	0.1486 ± 0.0012	0.1783 ± 0.0032	88.72	0.1749 ± 0.0016
Electrons	0.0148 ± 0.001	0.0198 ± 0.0006	9.86	0.0183 ± 0.0002
Photons	1.1053 x 10 <sup>-6</sup> ± 1.82 %	3.7904 x 10 <sup>-7</sup> ± 170.03 %	0.00	7.8355 x 10 <sup>-7</sup> ± 5.69 %
Protons	8.5832 x 10 <sup>-4</sup> ± 14.21 %	1.5021 x 10 <sup>-3</sup> ± 21.36 %	0.75	3.0876 x 10 <sup>-3</sup> ± 4.44 %
Alpha	3.4244 x 10 <sup>-4</sup> ± 15.08 %	4.6763 x 10 <sup>-4</sup> ± 59.71 %	0.23	9.3214 x 10 <sup>-4</sup> ± 6.61 %
<b>Total</b>	<b>0.1653 ± 0.0013</b>	<b>0.2009 ± 0.0031</b>	<b>100</b>	<b>0.2004 ± 0.0018</b>

[D]

1 MeV	Glass coverslip (1.9152 cm <sup>3</sup> )	Cell Monolayer (0.001 cm <sup>3</sup> )		Medium (water) (18.799 cm <sup>3</sup> )
Particles	Absorbed Dose (cGy)	Absorbed Dose (cGy)	Contribution to total dose %	Absorbed Dose (cGy)
Total heavy ions	0.1654 ± 0.0013	0.1971 ± 0.0038	98.30 0.15	0.1958 ± 0.0014
<sup>12</sup> C ions	0.1652 ± 0.0014	0.1910 ± 0.0038	98.15	0.1934 ± 0.0013
Electrons	5.0037 x 10 <sup>-7</sup> ± 73.15 %	7.0334 x 10 <sup>-7</sup> ± 83.07 %	0.00	1.7944 x 10 <sup>-6</sup> ± 26.38 %
Photons	3.2179 x 10 <sup>-7</sup> ± 101.49 %	0.0000 ± 0.0000	0.00	1.6590 x 10 <sup>-11</sup> ± 78.71 %
Protons	7.5727 x 10 <sup>-5</sup> ± 11.64 %	1.5147 x 10 <sup>-4</sup> ± 26.84 %	0.08	2.8089 x 10 <sup>-4</sup> ± 3.62 %
Alpha	3.4659 x 10 <sup>-4</sup> ± 16.25 %	6.5669 x 10 <sup>-4</sup> ± 0.0006	0.33	9.9823 x 10 <sup>-4</sup> ± 7.15 %
<b>Total</b>	<b>0.1670 ± 0.0014</b>	<b>0.2005 ± 0.0037</b>	<b>100</b>	<b>0.2010 ± 0.0013</b>

Errors represent standard deviations of the mean. When the standard deviation is <0.0001 cGy, it is expressed and noted in % as it can represent a high deviation. The term “total heavy ion” refers to the primary 290 MeV/u <sup>12</sup>C ions and the fragments.